Plotting methods for visualizing phylogenies & comparative data

Liam J. Revell

16 December 2016

Chapter 4
Graphical Methods for Visualizing Comparative Data on Phylogenies

Liam J. Revell

L. Z. Garamszegi (ed.), *Modern Phylogenetic Comparative Methods and Their Application in Evolutionary Biology*, DOI: 10.1007/978-3-662-43550-2_4,

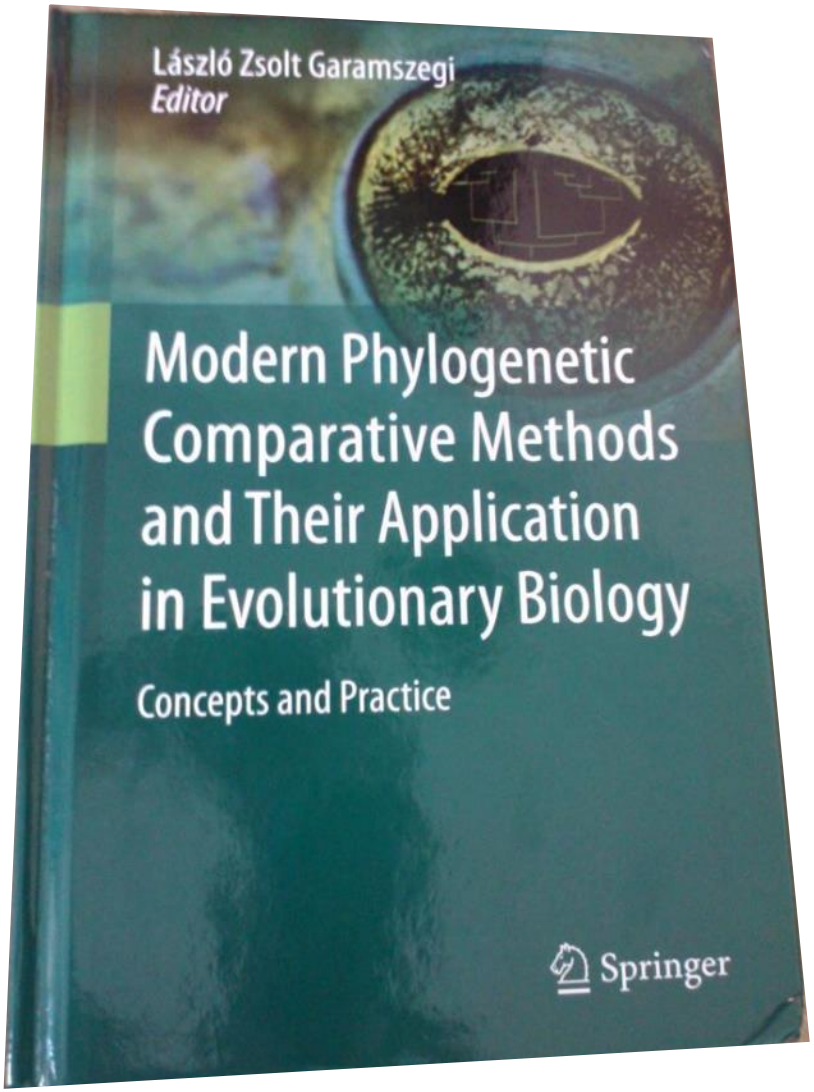

Plotting methods for phylogenies & comparative data

- Every introductory statistics course teaches us to *always plot our data*; however this is often overlooked in phylogenetic comparative studies. Why?

Plotting methods for phylogenies & comparative data

- Every introductory statistics course teaches us to *always plot our data*; however this is often overlooked in phylogenetic comparative studies. Why?
- Phylogenetic data are complex, and standard plotting methods are not appropriate – specialized methods are required.

Discrete character methods

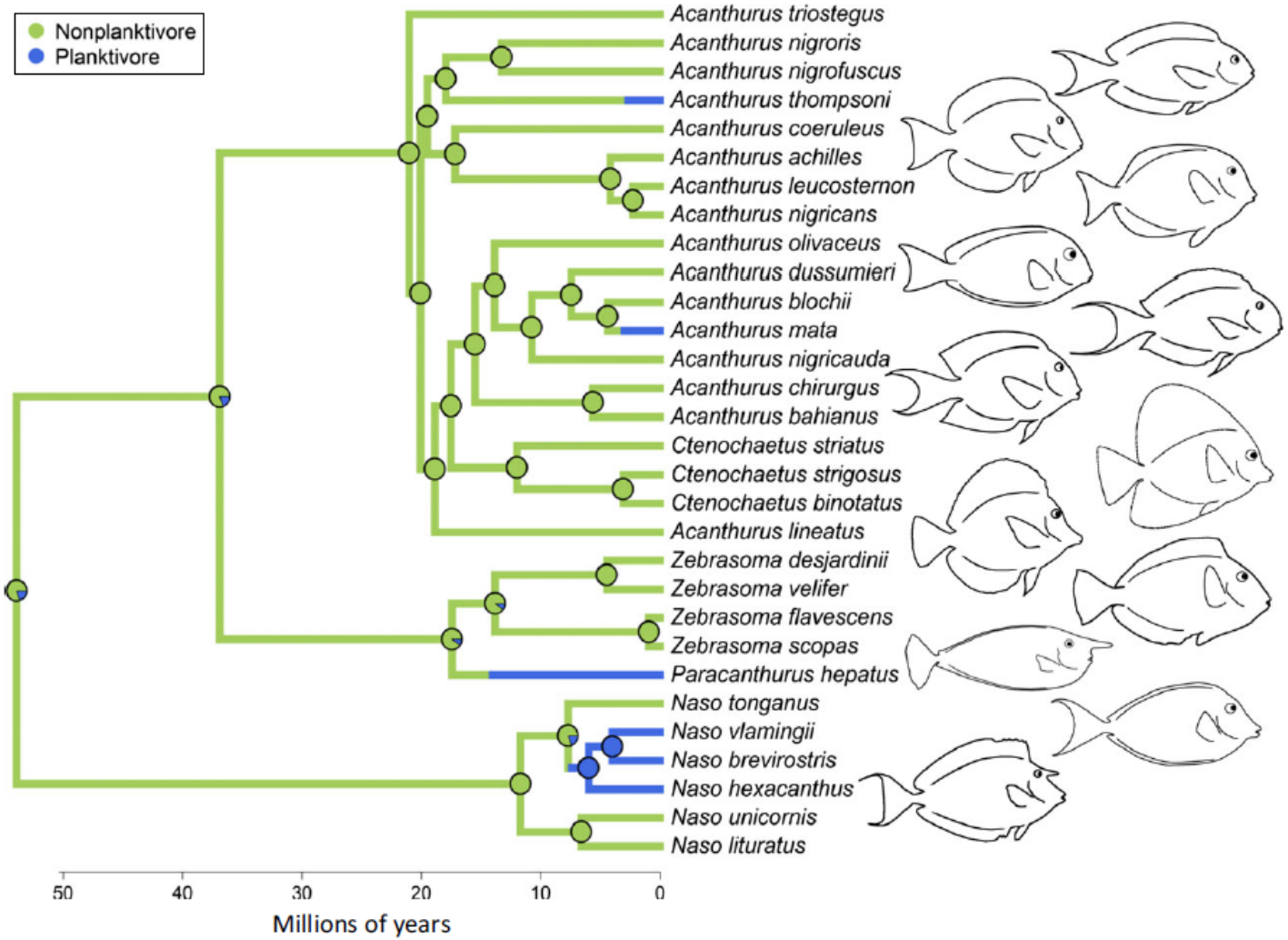

Fig. 1 Time-calibrated phylogeny (adapted from Sorenson *et al.*, 2013) of acanthurid species included in this study with a sample stochastic character map of diet and ancestral state estimates from 500 simmaps indicated at the nodes. Blue and green denote zooplanktivorous and nonzooplanktivorous species, respectively. Fish outlines illustrate morphological diversity within the clade and are identified as follows (from top to bottom): *Acanthurus thompsoni, A. blochii, A. leucosternon, A. mata, A. nigricauda, Ctenochaetus binotatus, Zebrasoma velifer, Z. flavescens, Paracanthurus hepatus, Naso brevirostris, N. lituratus* and *N. unicornis*.

(Friedman et al. 2016; *J. Evol. Biol.*)

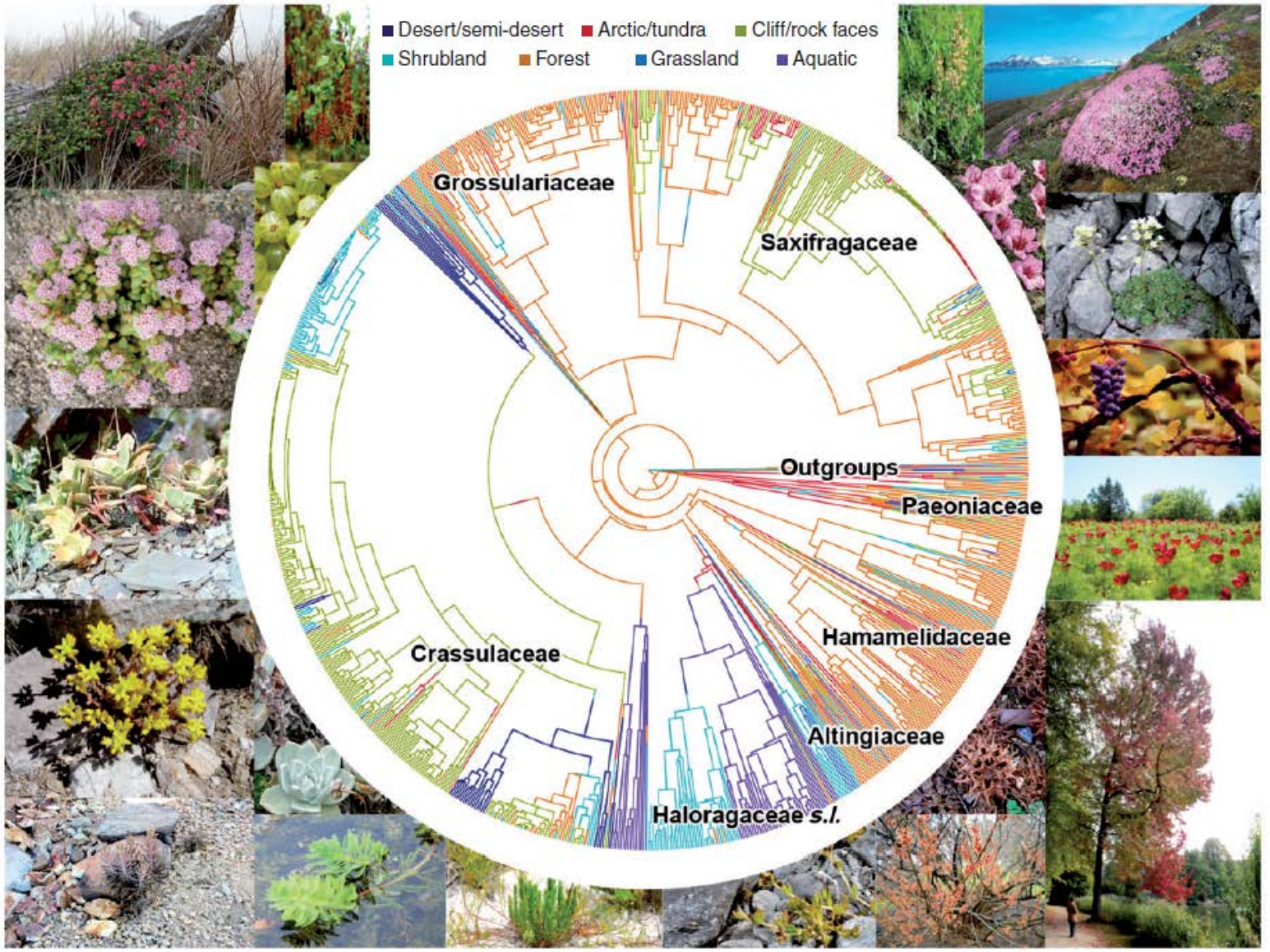

FIG. 1. A phylogenetic tree for species of Saxifragales with a reconstruction of habitat evolution using SIMMAP (see key for colours). Representatives of major sub-clades are shown around the tree near the corresponding family name.

(de Casas et al. 2016; *Ann. Bot.*)

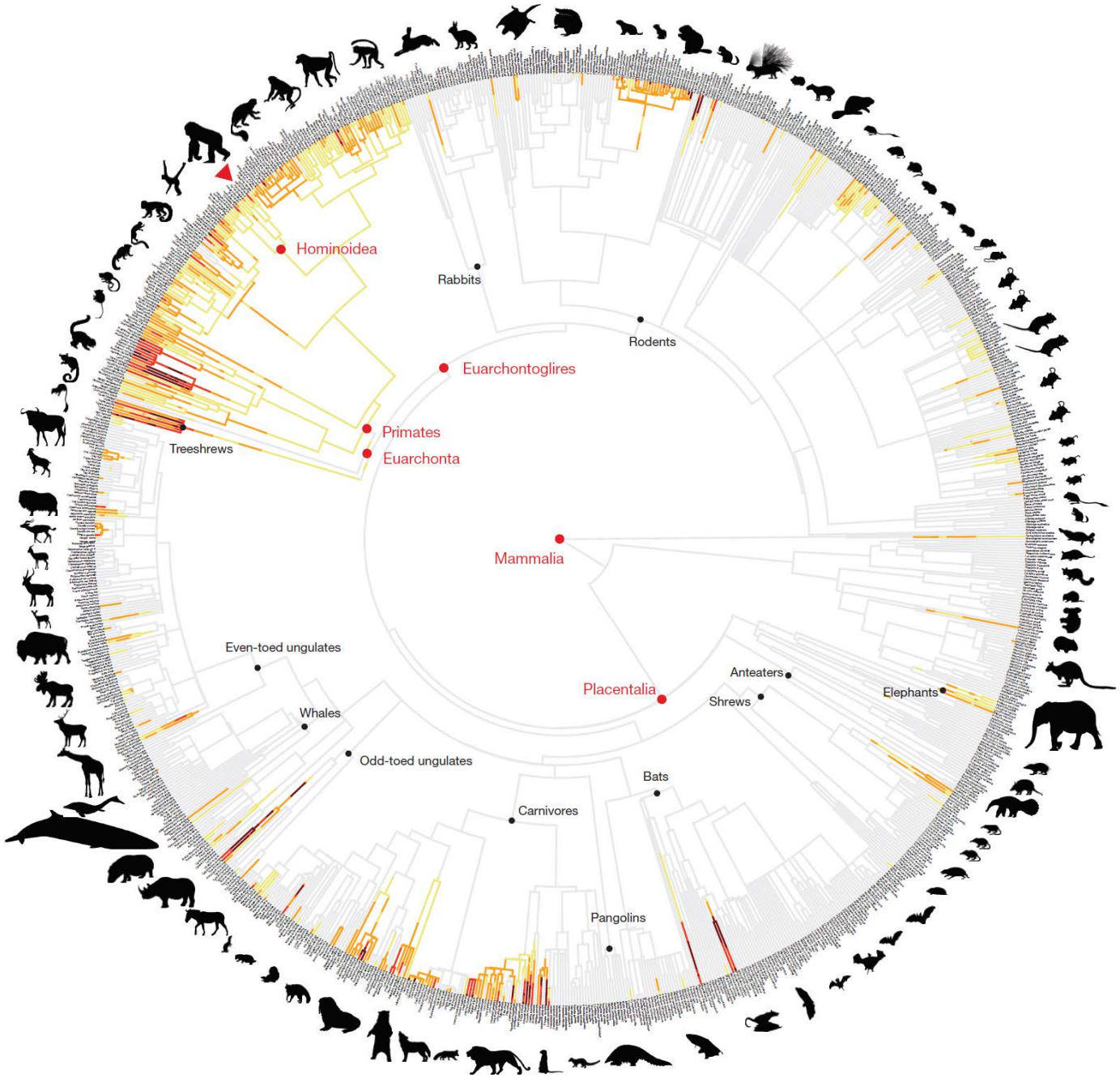

Figure 1 | Evolution of lethal aggression in non-human mammals. Tree showing the phylogenetic estimation of the level of lethal aggression in mammals ($n = 1{,}024$ species) using stochastic mapping. Lethal aggression increases with the intensity of the colour, from yellow to dark red. Light grey indicates the absence of lethal aggression. Mammalian ancestral nodes compared with human lethal violence are shown in red, whereas main placental lineages are marked with black nodes. The red triangle indicates the phylogenetic position of humans. The silhouettes of representative mammals (downloaded from http://www.phylopic.org) illustrate the main mammalian clades. They are licenced for use in the Public Domain without copyright, except for the silhouettes of Murinae (D. Liao), *Jaculus* (M. Karaka), *Philander* (S. Werning), *Rattus* (R. Groom), *Molossus* (Zimices), *Balaenoptera* (C. Hoh), *Rousettus* (O. Peles), *Connochaetes*, *Redunca*, and *Kobus* (J. A. Venter, H. H. T. Prins, D. A. Balfour and R. Slotow), that are licenced under a Creative Commons 3.0 license (http://creativecommons.org/licenses/by/3.0).

(Gómez et al. 2016; *Nature*)

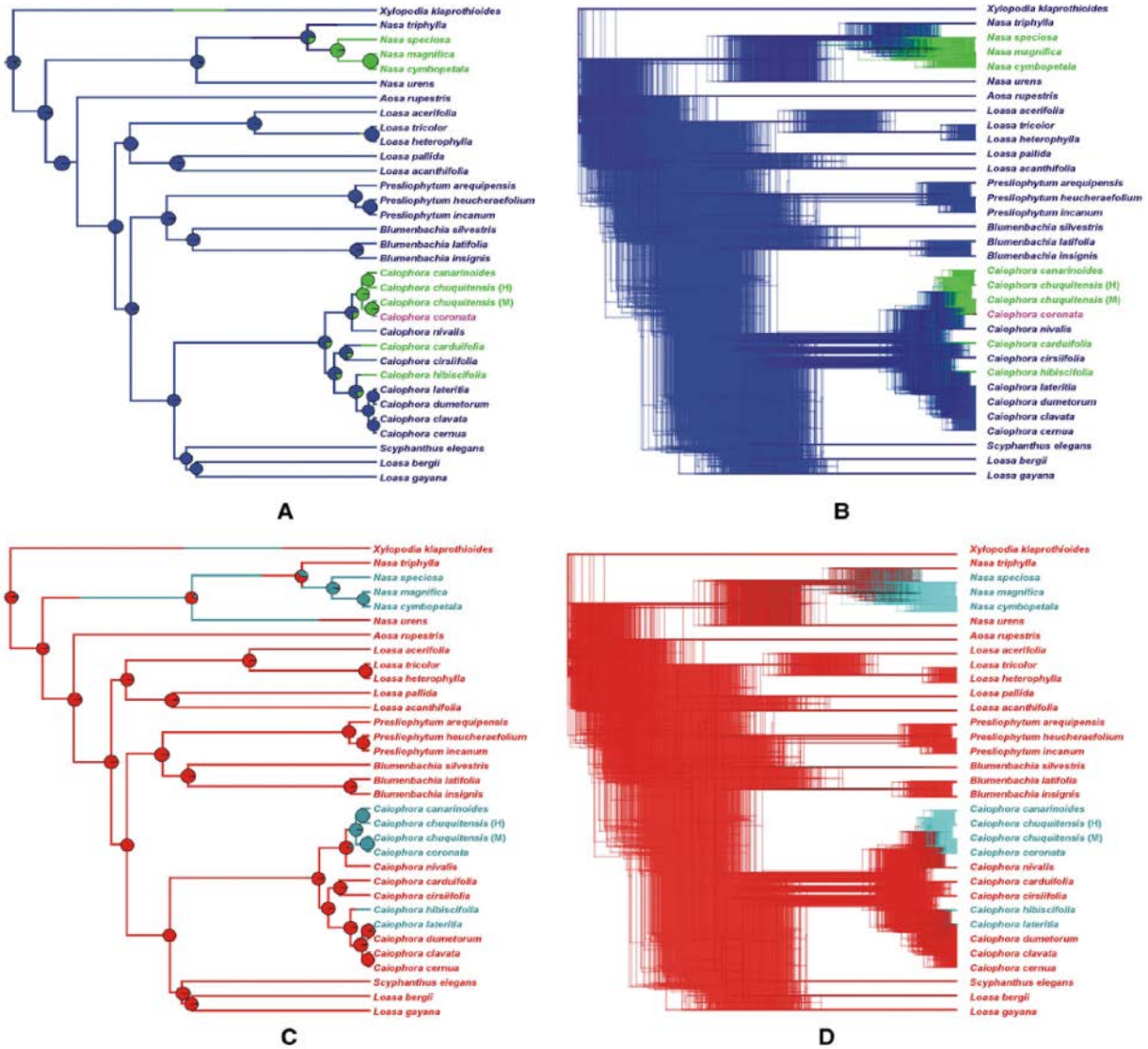

Fig. 2 Stochastic character mappings of **a**, **b** the pollinator and **c**, **d** the flower phenotype. Pollination strategies and flower phenotype are indicated with *colours*. Pollination strategy: *blue* = bee pollination; *green* = hummingbird pollination; *purple* = rodent pollination; flower phenotype: *red* = TRF; *cyan* = FRF. *Panels A* and *C* show the maximum credibility tree with pie charts on its nodes, indicating the posterior probability of **a** each pollination strategy and **c** each flower phenotype retrieved by 1000 stochastic character mappings. *Panels B* and *D* show the superimposition of 1000 phylogenetic trees, with 10 stochastic character mappings each. (Color figure online)

(Strelin et al. 2016; *Evol. Ecol.*)

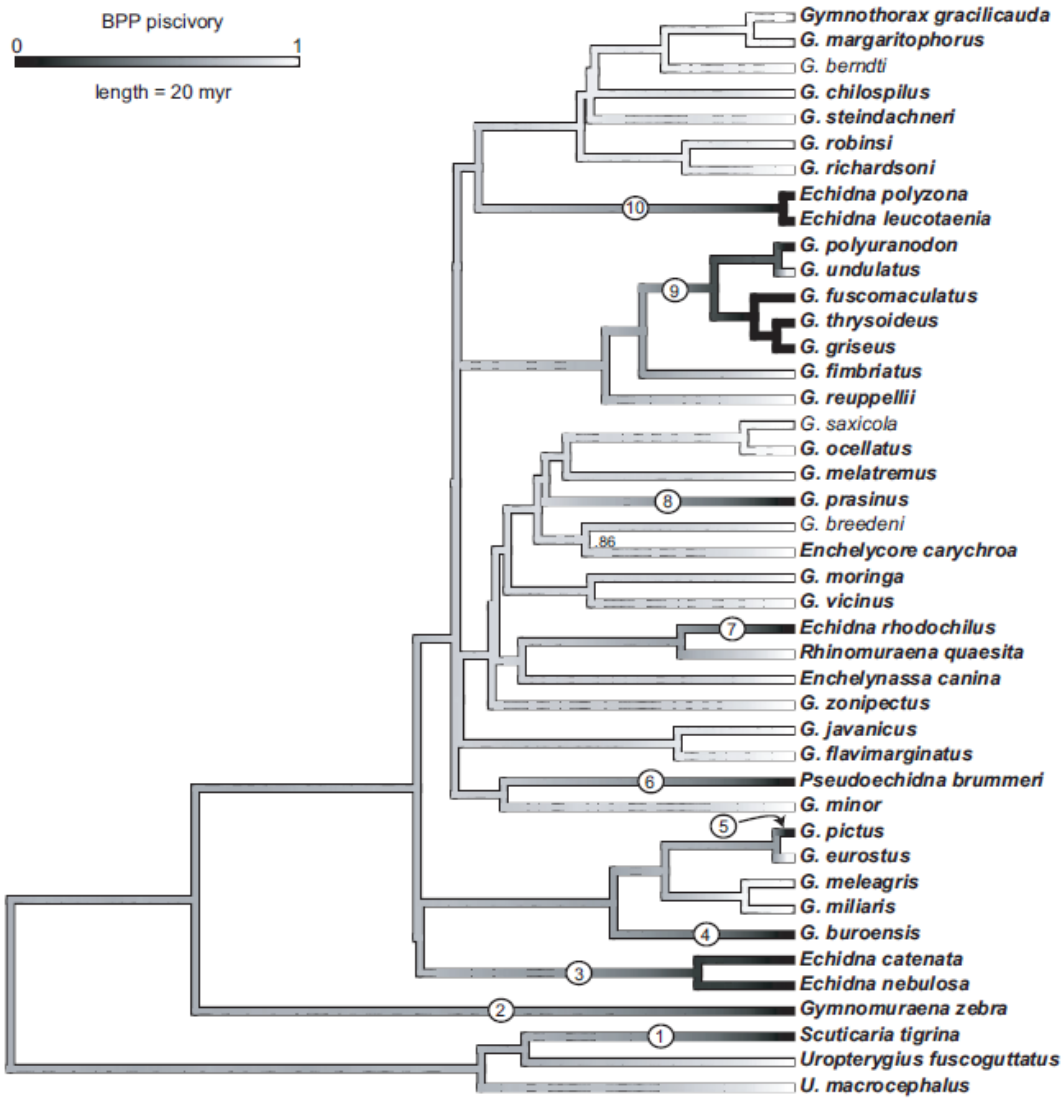

Figure 1: Summary of stochastic diet maps on the maximum clade credibility phylogeny for 43 moray eel species. Branch lengths are given in millions of years (My); scale bar shown in the upper left inset. Nodes receive 0.90 or greater Bayesian posterior probability (BPP) support unless otherwise indicated. Species names in bold are those included in our morphological data set. Shading on branches represents BPP of piscivory for branch segments across 1,000 stochastic character maps. White indicates that the BPP of piscivory equals 1, and darker shading corresponds with lower BPP of piscivory and therefore higher BPP of durophagy. We inferred 10 durophagous transitions, identified by encircled numbers. Transitions were determined to occur along branches on which ancestral nodes are light gray (favoring piscivory), and descendant nodes are dark gray or black (favoring durophagy). Note that the positioning of numbers along branches is arbitrary and not meant to suggest specific timing of transitions. This figure was generated using the phytools function densityMap (Revell 2012, 2013).

(Collar et al. 2014; *Am. Nat.*)

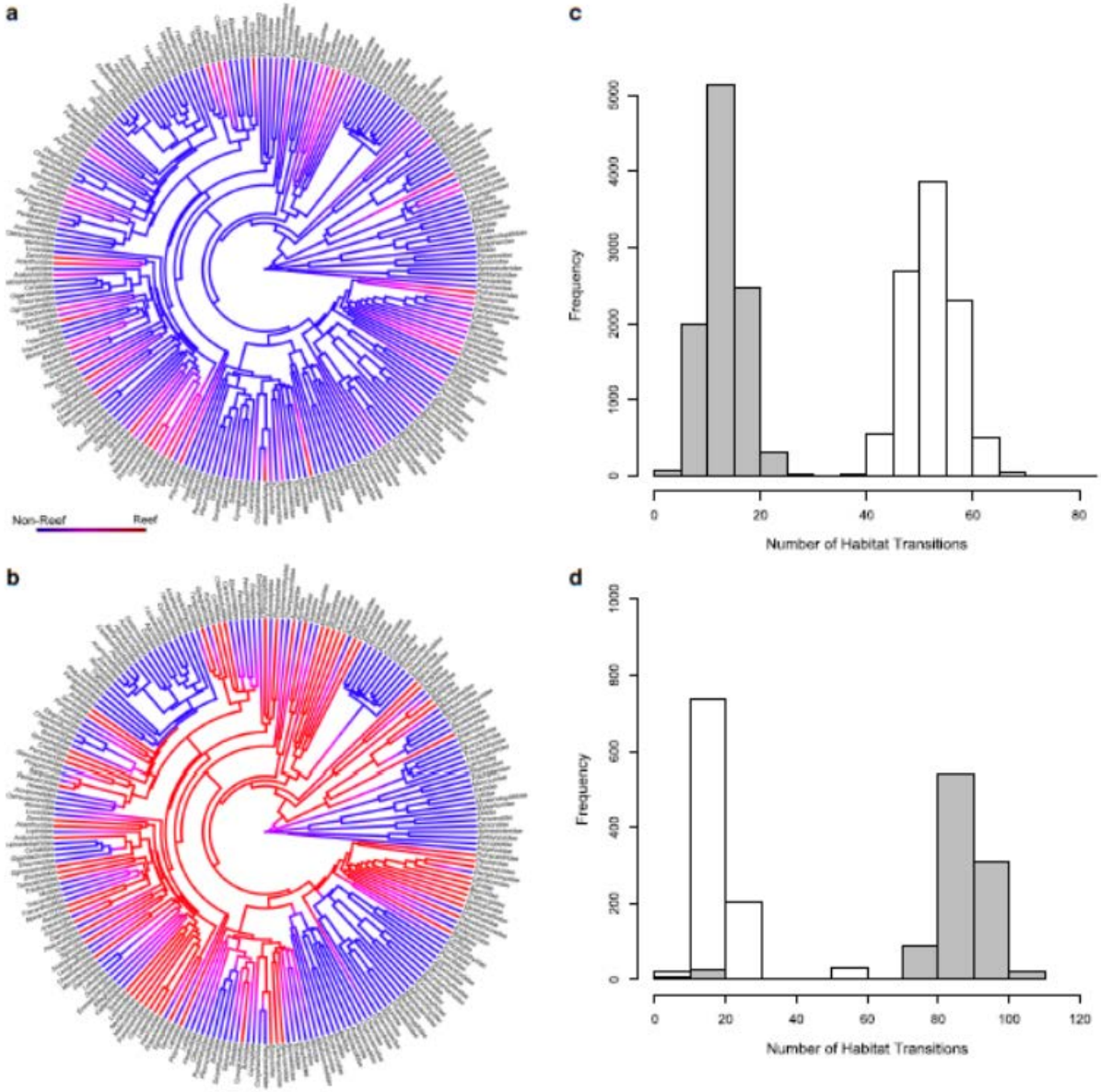

Fig. 1 Reconstructed history of reef living according to **a** the percentage of extant species living on reefs given in FishBase **b** classification of Bellwood and Wainwright (2002). *Color* gradation represents the posterior probability of reef (*red*) or non-reef (*blue*) ancestry according to 1000 stochastic character maps on the maximum clade credibility phylogeny from Near et al. (2013) converted to the family level. Histograms of the number of habitat transitions from non-reef to reef (*gray*) and from reef to non-reef (*white*) according to **c** the percentage of extant species living on reefs given in FishBase **d** classification of Bellwood and Wainwright (2002), calculated from the 1000 stochastic character maps

(Price et al. 2015; *Coral Reefs*)

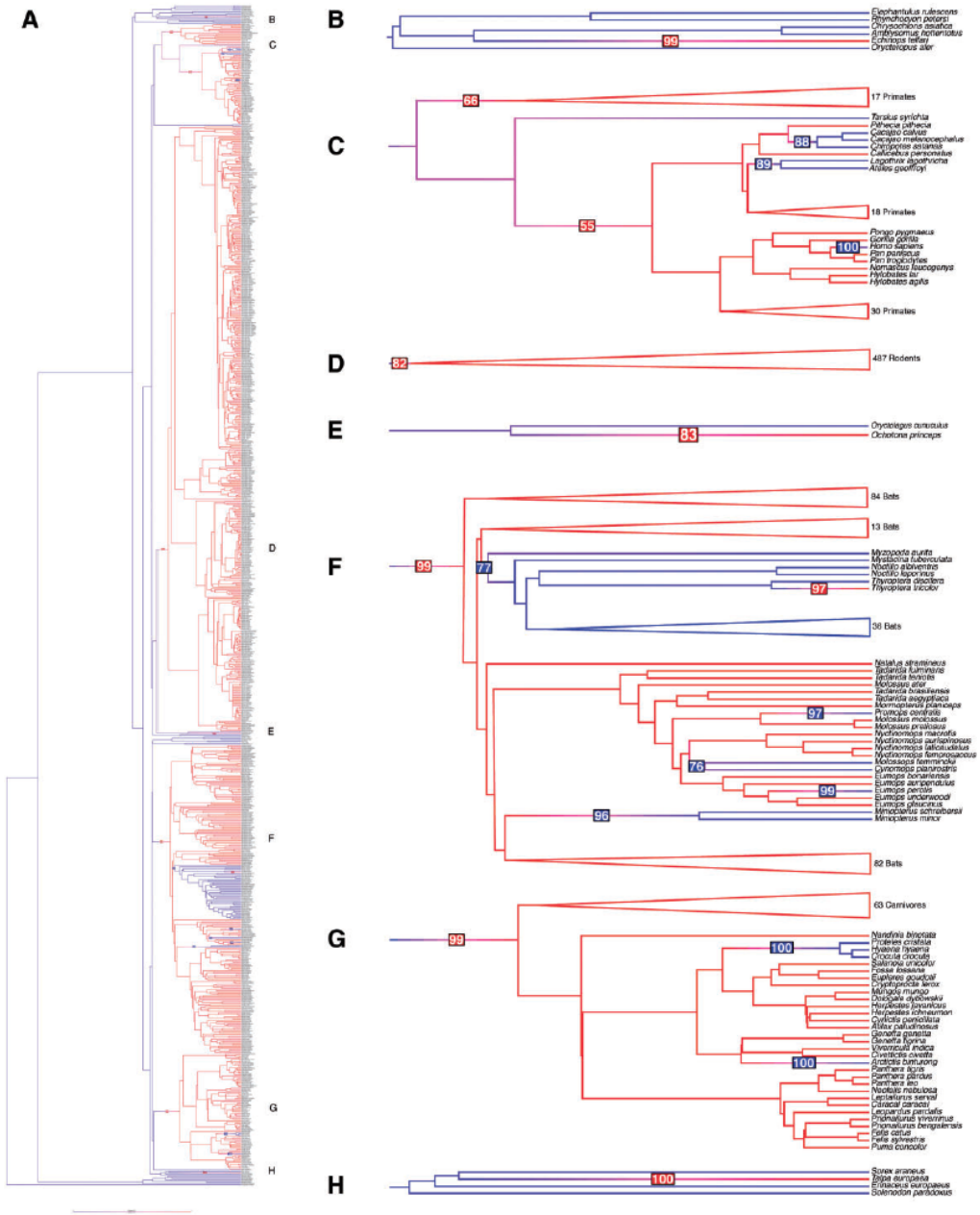

Fig. 1 **(A)** High confidence gains and losses of the baculum derived from stochastic mapping. Red branches indicate species with a baculum, blue without; numbers in red (blue) boxes indicate the proportion of iterations that mapped a baculum gain (loss) to those particular branches. Branches where a transition occurred in at least 50% of the iterations are highlighted in **(B)**–**(H)**, which correspond to regions labeled **B**–**H** in panel A. Fig. 1A is meant to give an overall impression of the distribution of bacula across mammals; a zoomable version is provided as Supplementary Figure 1.

(Schultz et al. 2016; *ICB*)

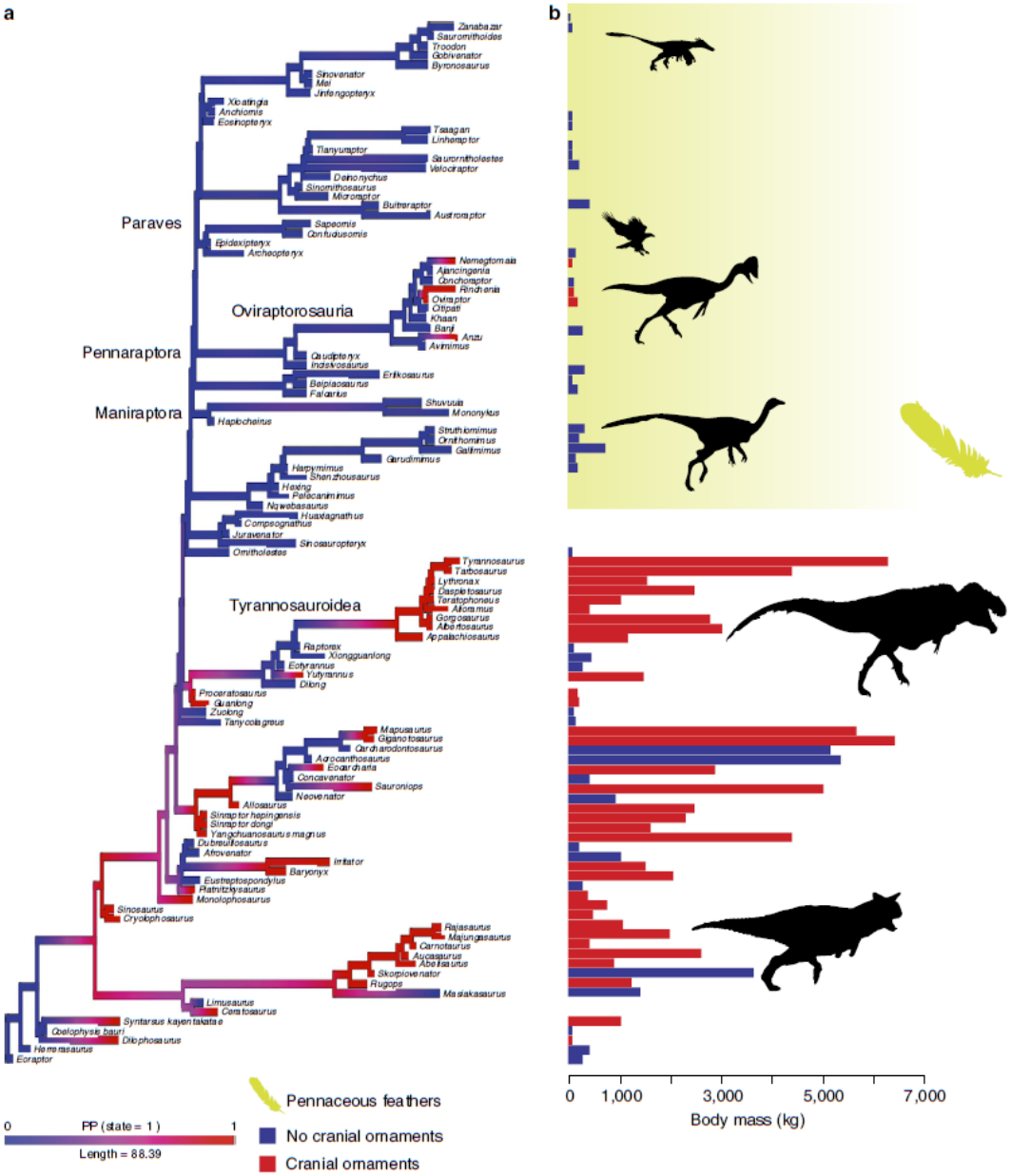

Figure 2 | Phylogeny of non-avian theropods used in this study. (**a**) Density map of Bayesian stochastic character probabilities of unornamented (blue) and ornamented (red) character states. (**b**) Body mass estimates for non-avian theropods used in this study. Green shading shows the distribution of pennaceous feathers among theropods.

(Gates et al. 2016; *Nature Communications*)

Continuous character methods

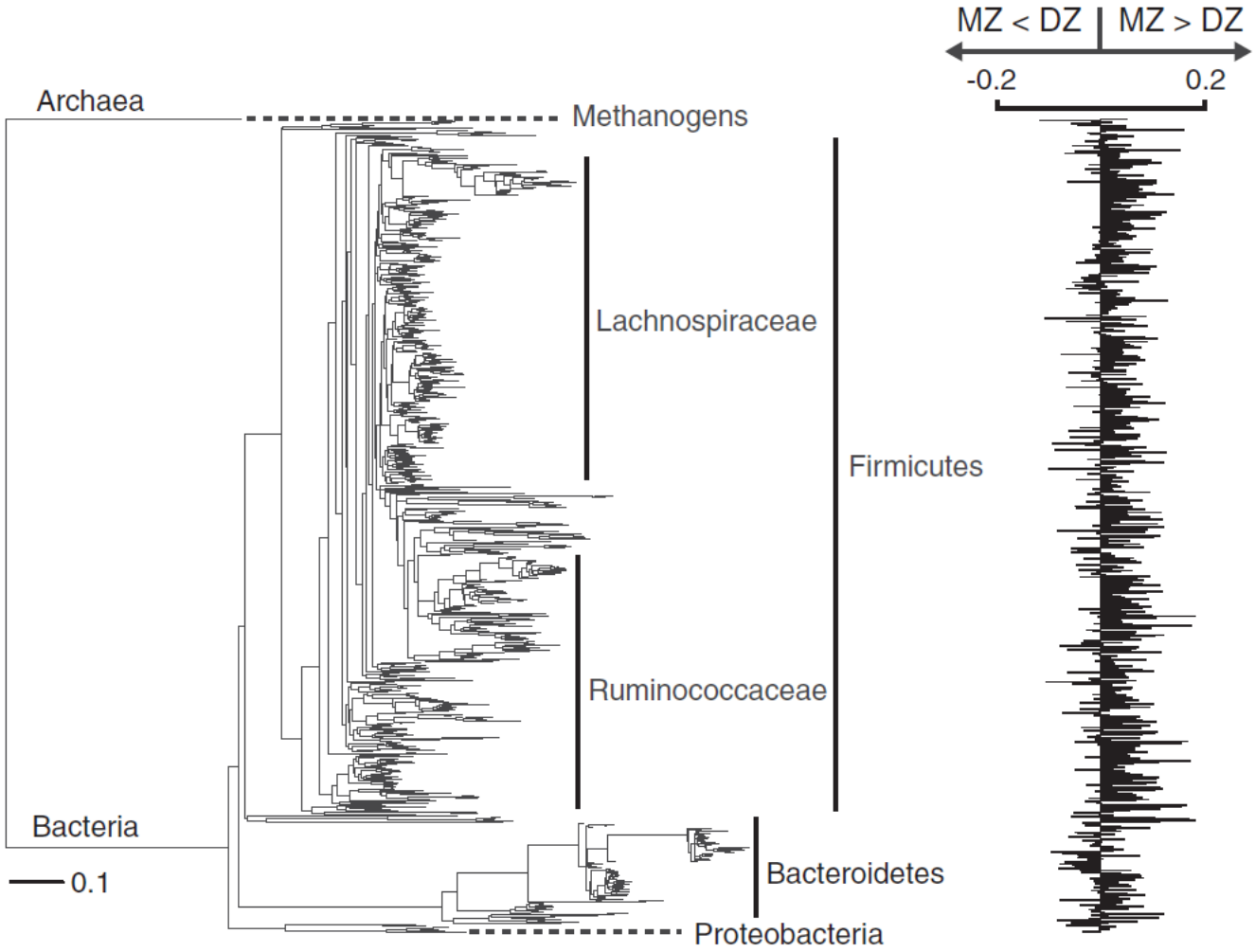

Figure 2. OTU Relative Abundances Are More Highly Correlated within MZ Than DZ Twin Pairs

Left: a phylogeny of taxa in the TwinsUK study (Greengenes tree pruned to include only OTUs shared by 50% of the TwinsUK participants).

Right: corresponding twin-pair intraclass correlation coefficients (ICCs). ICCs were calculated for each OTU and the difference in correlation coefficients for MZ twin pairs versus DZ twin pairs. Bars pointing to the right indicate that the difference is positive (i.e., MZ ICCs > DZ ICCs) and bars pointing to the left indicate negative differences (DZ ICCs > MZ ICCs). The scale bar associated with the phylogeny shows substitutions/site.

See also Figure S2.

(Goodrich et al. 2014; *Cell*)

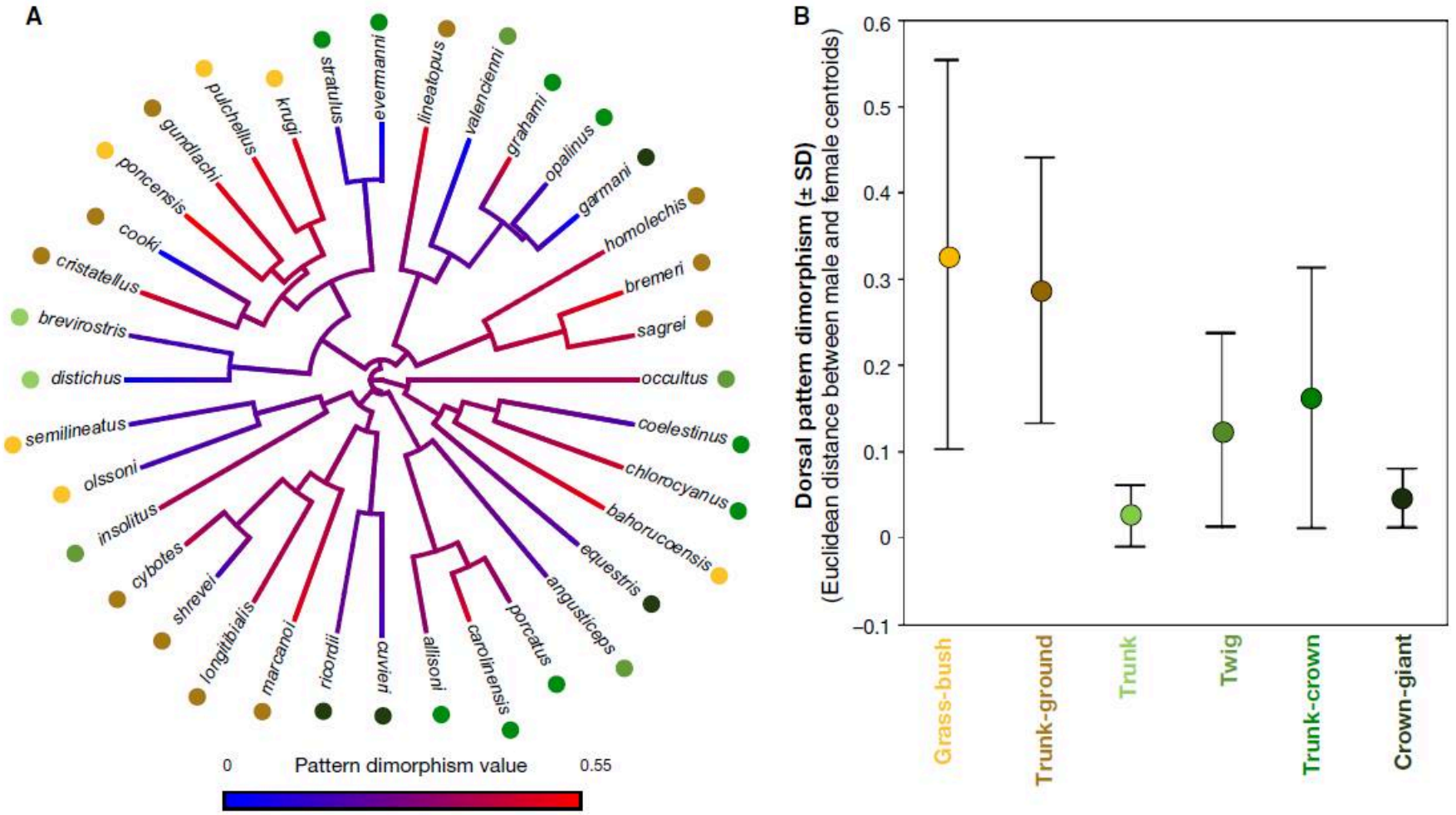

Figure 2. Association between sexual dimorphism in dorsal pattern and ecomorph in 36 species of *Anolis*. A, Phylogenetic tree with coloured branches representing values of dimorphism in dorsal pattern (Euclidean distance). Circles at tips represent ecomorph and the colour legend is the same as in (B). B, Values of dorsal pattern dimorphism according to ecomorph class.

(Medina et al. 2016; *B. J. Linn. Soc.*)

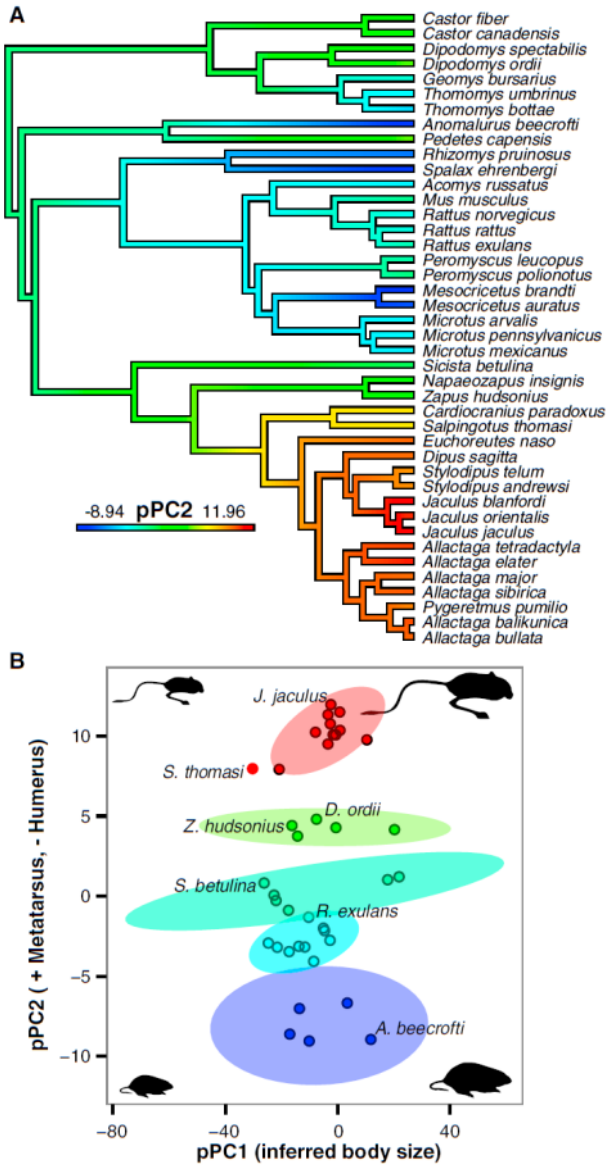

Figure 4. Phylogenetically Corrected Principal Components Analysis Illustrates Major Proportional Differences across Rodent Limbs

(A) pPC2 is mapped as a continuous trait on the phylogeny of rodents with ancestral states reconstructed (graded color).

(B) Clusters of similar ecomorphs plotted with respect to pPC1 (representing variation due to body size; 90.9% of the total variance) and pPC2 (representing degree and direction of limb specialization; 86.1% of remaining variance with pPC1 removed). Shaded ellipses demark the 95% confidence interval of each cluster.

(Moore et al. 2015; *Curr. Biol.*)

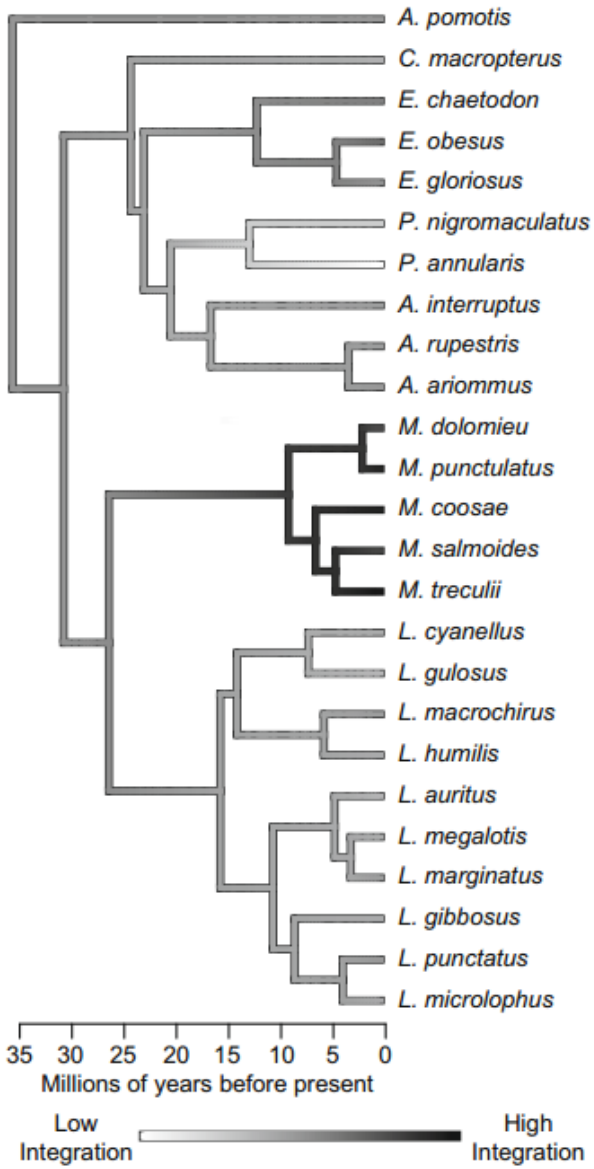

Fig. 3 Level of integration exhibited by each centrarchid species. Contour map phylogeny with high levels of integration represented by *darker colors*, and low levels of integration represented by *lighter colors*. Phylogeny produced with the R package *Phytools* using the *contMap* function (Revell 2012)

(Smith et al. 2015; *Evol. Biol.*)

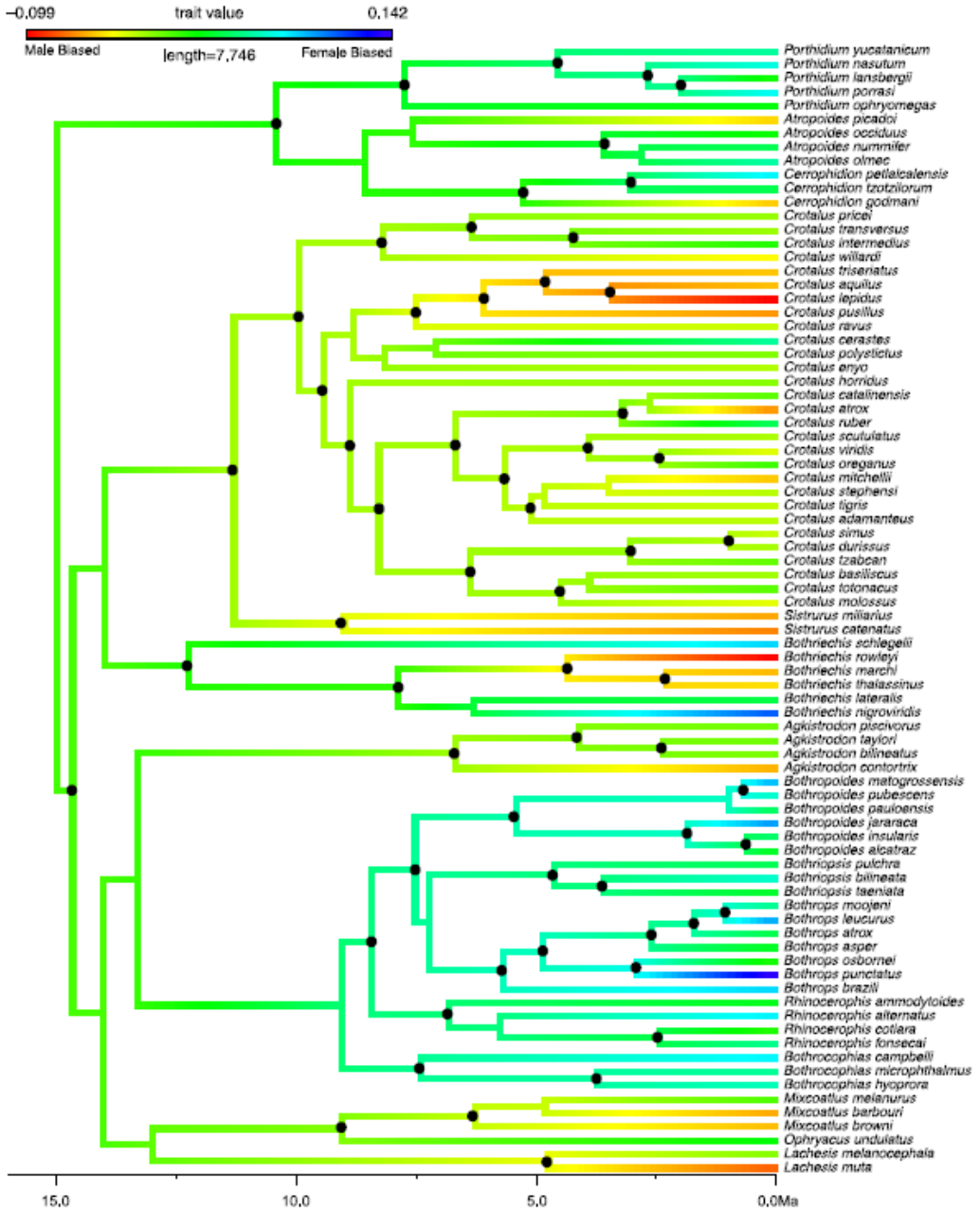

Fig. 1 Phylogeny of 82 species of NW crotalines, with branches coloured/shaded by ratio SSD values. SSD was reconstructed onto the phylogeny using the contMap function of the 'phytools' package (Revell, 2012) in R 2.15.2 (R Development Core Team, 2012). Red/white and blue/black coloration corresponds to the extremes of male-biased and female-biased SSD, respectively. Black circles indicate nodal support > 95% (see Appendix S3 for all support values).

(Hendry et al. 2014; *J. Evol. Biol.*)

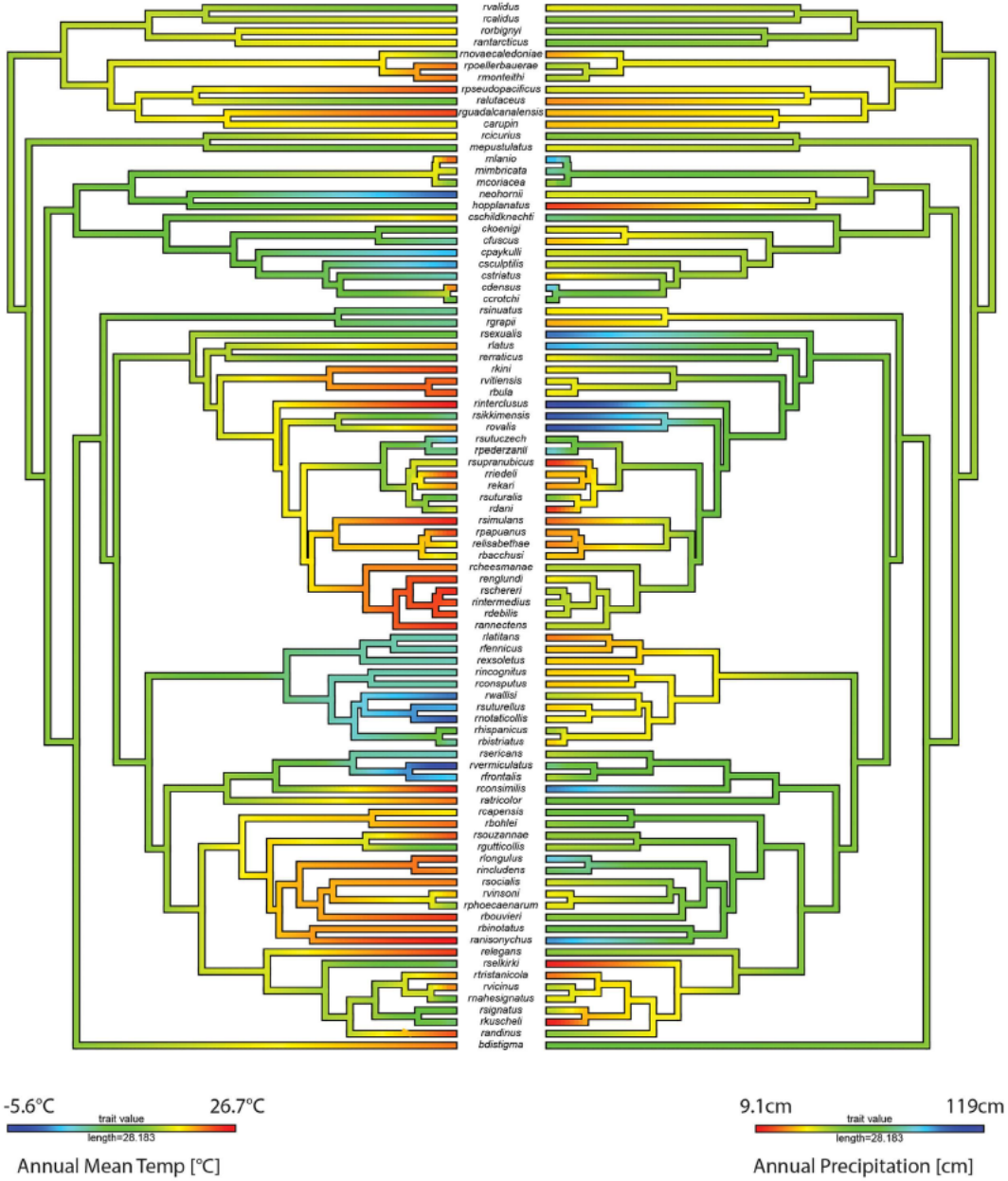

Figure 3. Ancestral climate preferences (annual mean temperature [°C] and annual precipitation [cm]) reconstructed using the '*contMap*' function in the *phytools* R package.

(**Morinière** et al. 2016; *Sci. Reports*)

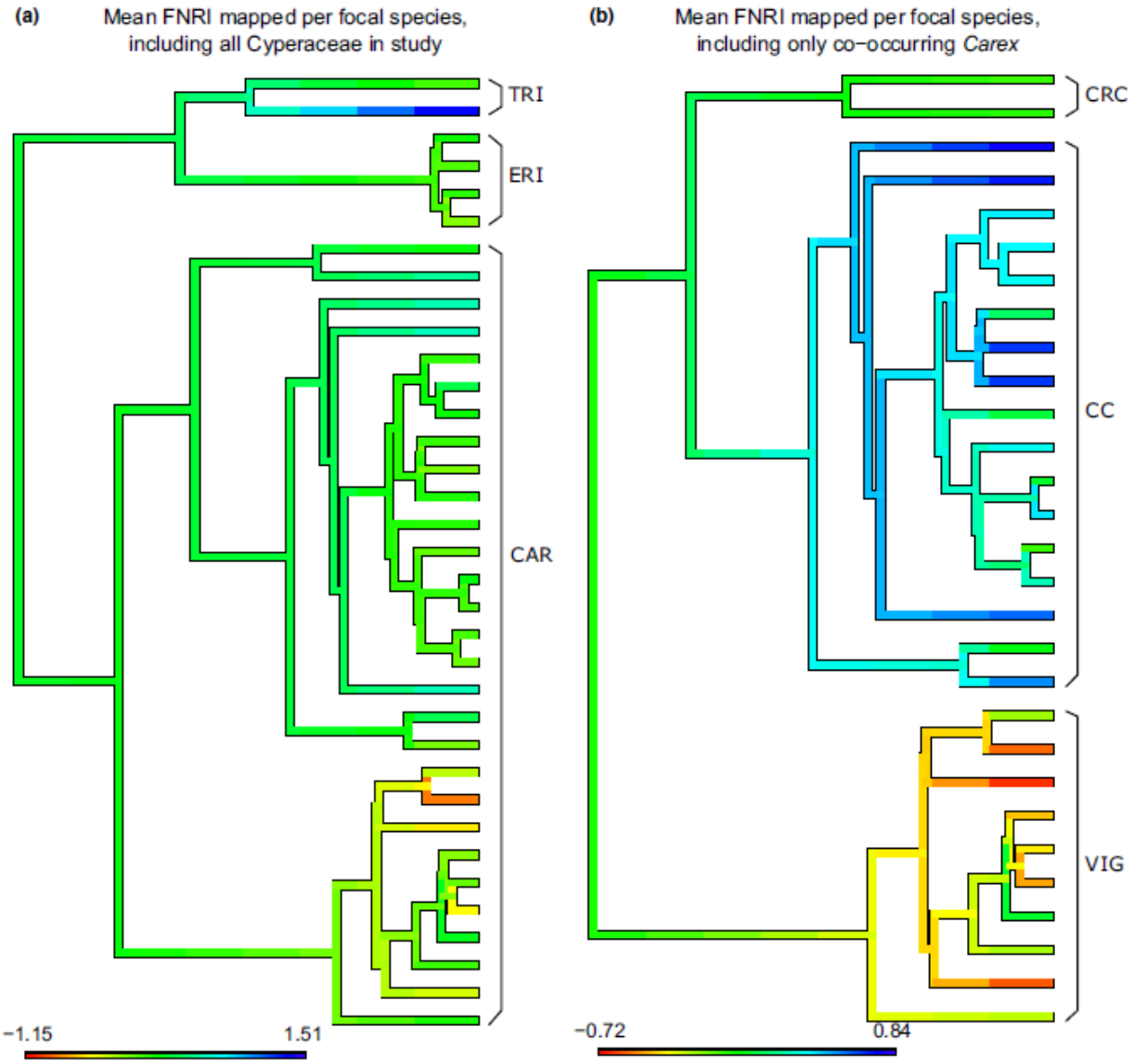

Fig. 2. Mean FNRI values mapped per focal species weighted by percentage cover estimates for (**a**) all co-occurring Cyperaceae in the study and (**b**) only co-occurring *Carex*. Mean values were mapped onto one of 100 randomly chosen phylogenies from the Bayesian posterior distribution using the contMap function available in the phytools package (Revell 2012) of R and are for illustration only. Blue colouring represents focal species with higher FNRI, whereas red colouring represents focal species with lower FNRI values. The colour bar in the bottom left hand corner of each phylogeny gives the scale of FNRI values and corresponding colours for each phylogeny. Abbreviations for each clade are the same as those in Appendix S4. Phylogenetic over-dispersion in the *Vignea* clade and phylogenetic clustering in the Core *Carex* clade became more evident when the species pool was narrowed to only co-occurring *Carex*.

(Elliot et al. 2016; *J. Veg. Sci.*)

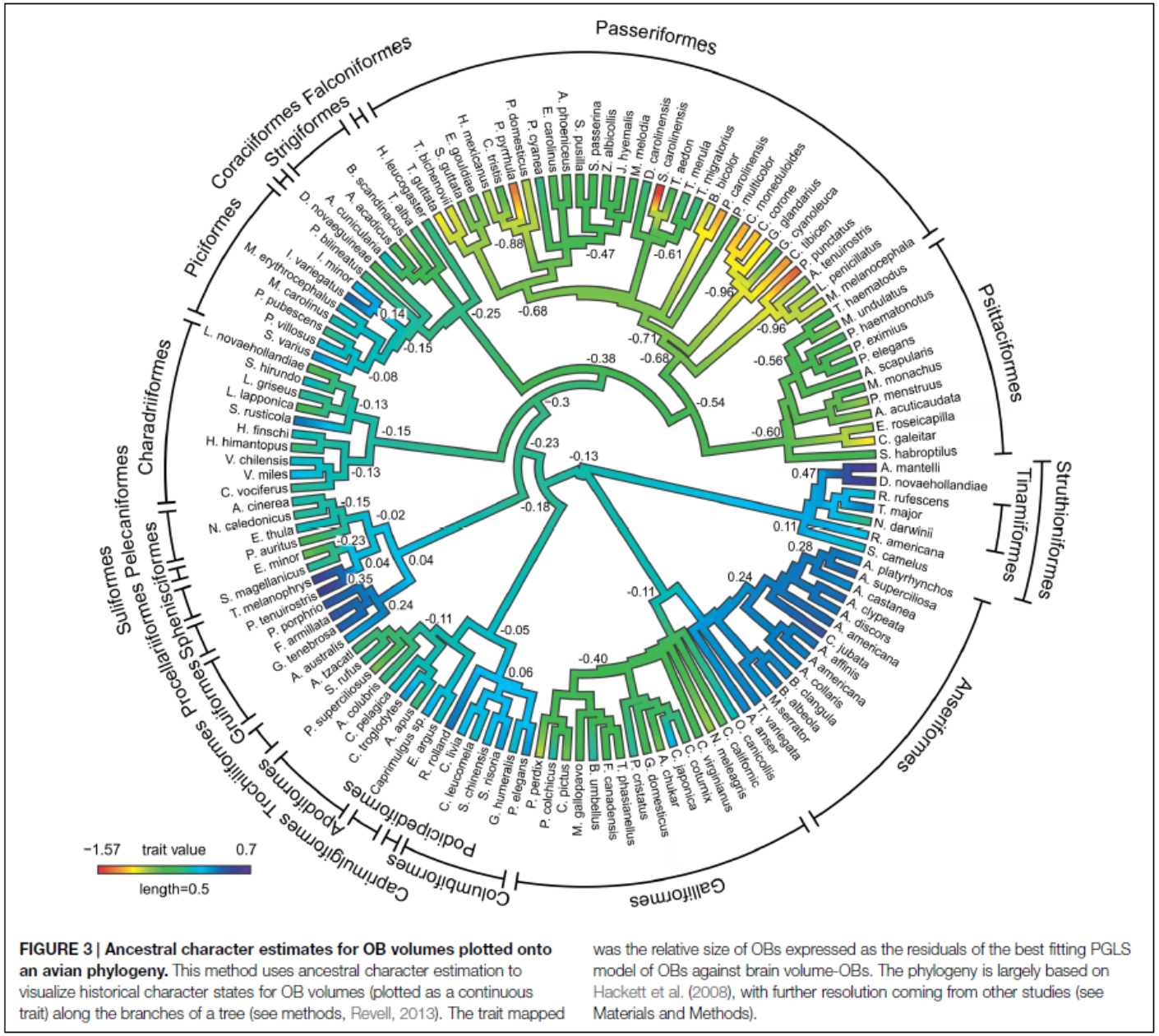

FIGURE 3 | Ancestral character estimates for OB volumes plotted onto an avian phylogeny. This method uses ancestral character estimation to visualize historical character states for OB volumes (plotted as a continuous trait) along the branches of a tree (see methods, Revell, 2013). The trait mapped was the relative size of OBs expressed as the residuals of the best fitting PGLS model of OBs against brain volume-OBs. The phylogeny is largely based on Hackett et al. (2008), with further resolution coming from other studies (see Materials and Methods).

(Cornfield et al. 2015; *Frontiers Neuroanat.*)

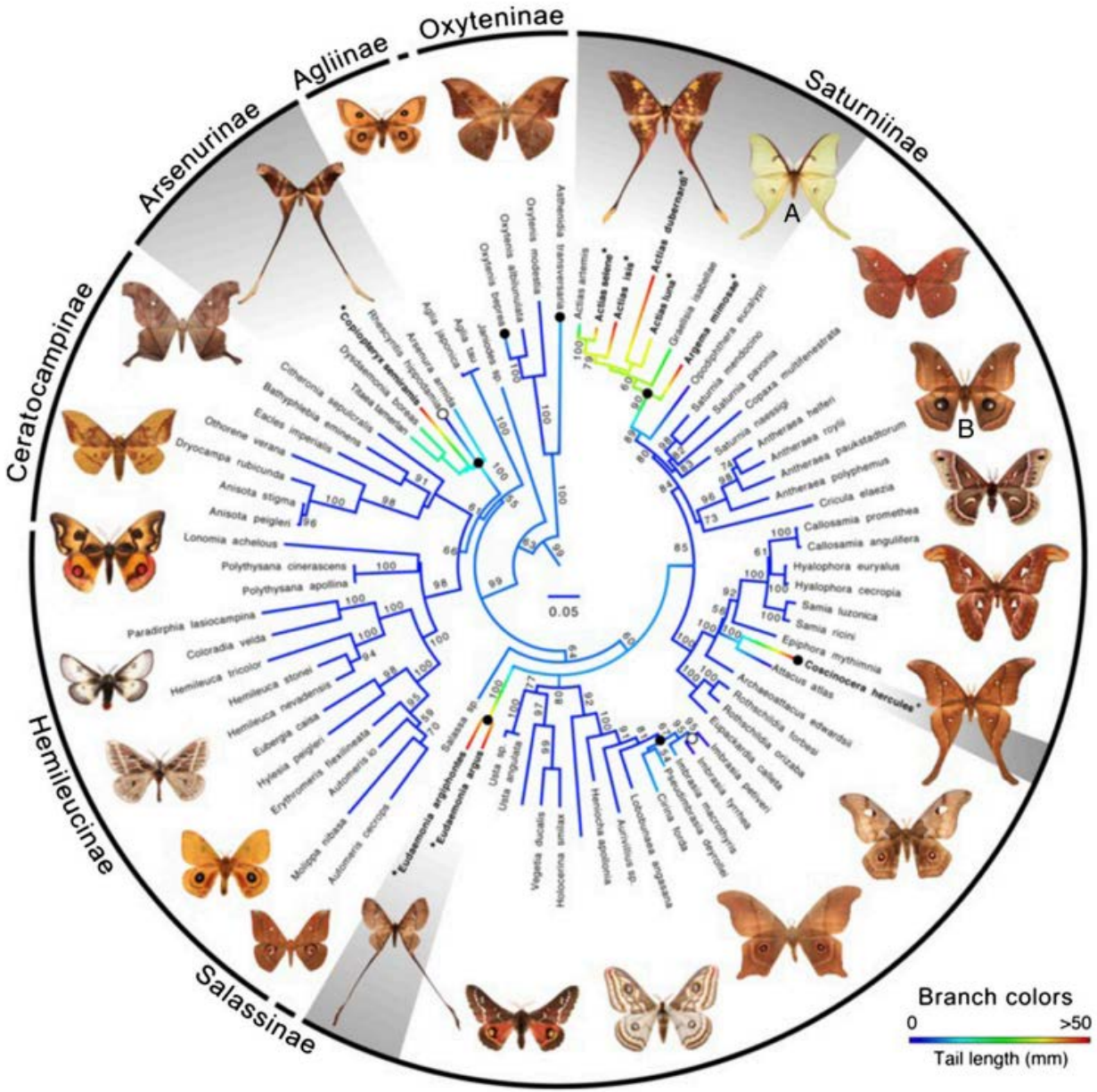

Fig. 2. ML molecular phylogeny of saturniid moths showing multiple independent origins of hindwing tails. Filled black circles indicate origin of tails. Open circles indicate losses. Branch colors indicate length of hindwing tail from absent (blue) to >50 mm (red), based on Phytools continuous character evolution analyses. Numbers by branches are bootstrap values. Gray shading denotes groups that have spatulate tails and contain species with tail lengths greater than 37.5 mm (the average for *A. luna*, $n = 10$). The images of saturniid moths used in these experiments are labeled: (A) *A. luna* and (B) *A. polypheumus*. Bold type and asterisks denote species that have tails longer than 37.5 mm. In combination with our bat–moth interaction data, this phylogeny suggests that tails serving a clear anti-bat function have evolved 4 times. Three additional origins of very short tails, of uncertain function, are also apparent.

(Barber et al. 2015; *PNAS*)

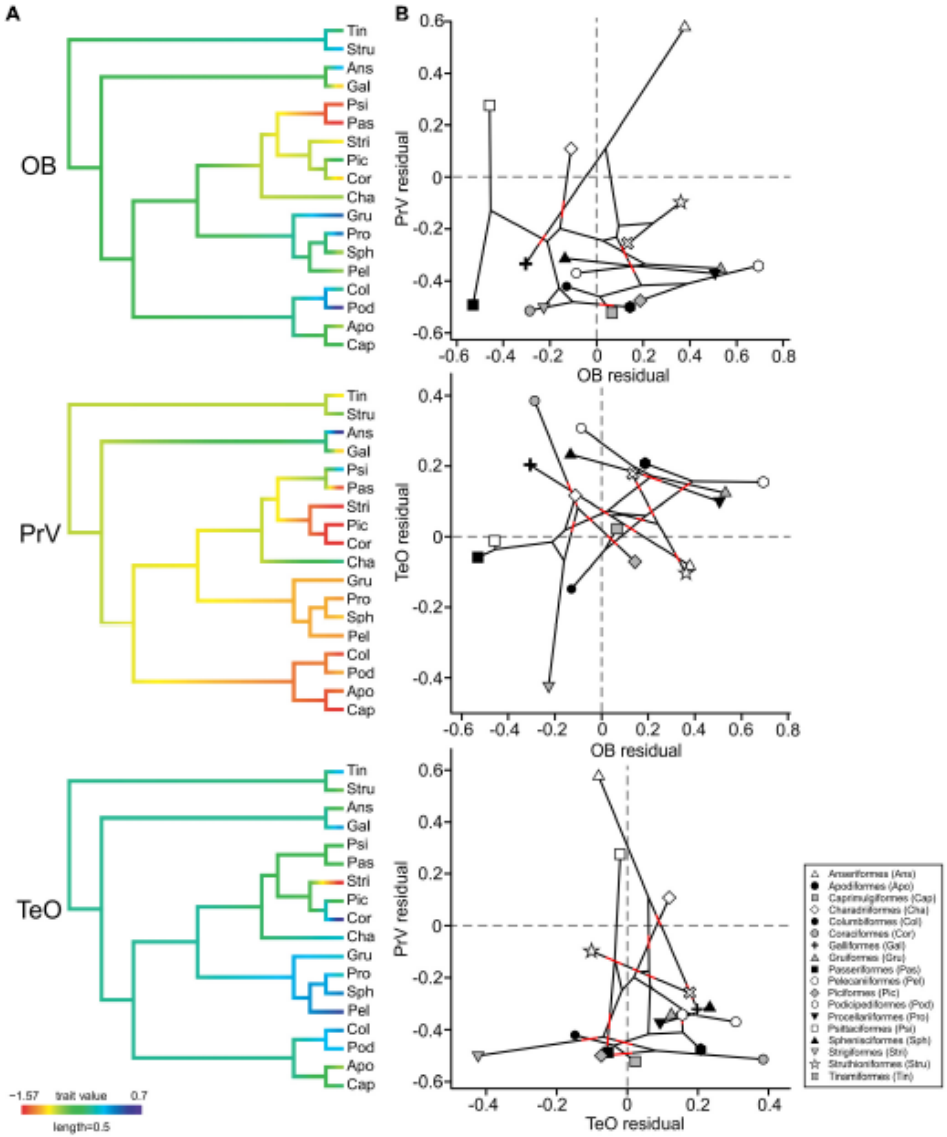

FIGURE 5 | Ancestral character estimates and residual plots for the OBs, the principal sensory nucleus of the trigeminal nerve (PrV), and the optic tectum (TeO). (A) Ancestral character estimates are plotted using the order averages for the relative size (expressed as the residuals of the best fitting PGLS model of each area against brain volume) of each sensory area (OB, PrV, and TeO) and are mapped onto the phylogeny based on Hackett et al. (2008). **(B)** Plots showing each sensory area plotting against the other while indicating the phylogenetic relationship of species (black lines). Red lines have been added to areas where the lines cross to allow for the tree branches to be more easily identified.

(Cornfield et al. 2015; *Frontiers Neuroanat.*)

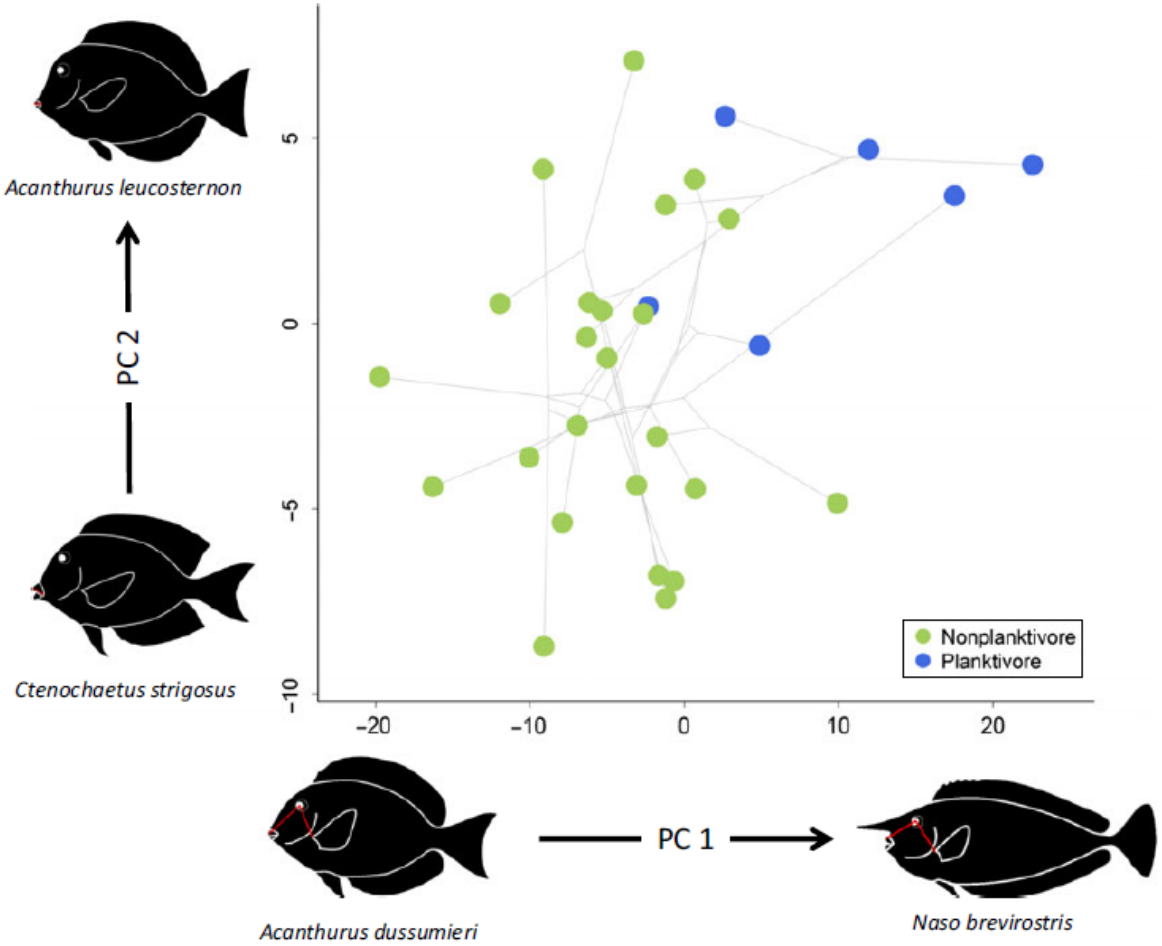

Fig. 2 Phylomorphospace projection of acanthurid species on the first two principal components. Blue and green circles denote zooplanktivorous and nonzooplanktivorous species, respectively. Fish silhouettes illustrate the outlying species on each axis, whereas superimposed red lines designate the traits loading high (> 0.82) on that Principal component (PC) and, therefore, the major sources of variation along that axis. PC1 scores are negatively correlated with adductor mandibulae mass, distances between eye and pectoral fin, and distances between eye and anterior tip of the premaxilla. PC2 scores load negatively with gill raker length (Table 1).

(Friedman et al. 2016; *J. Evol. Biol.*)

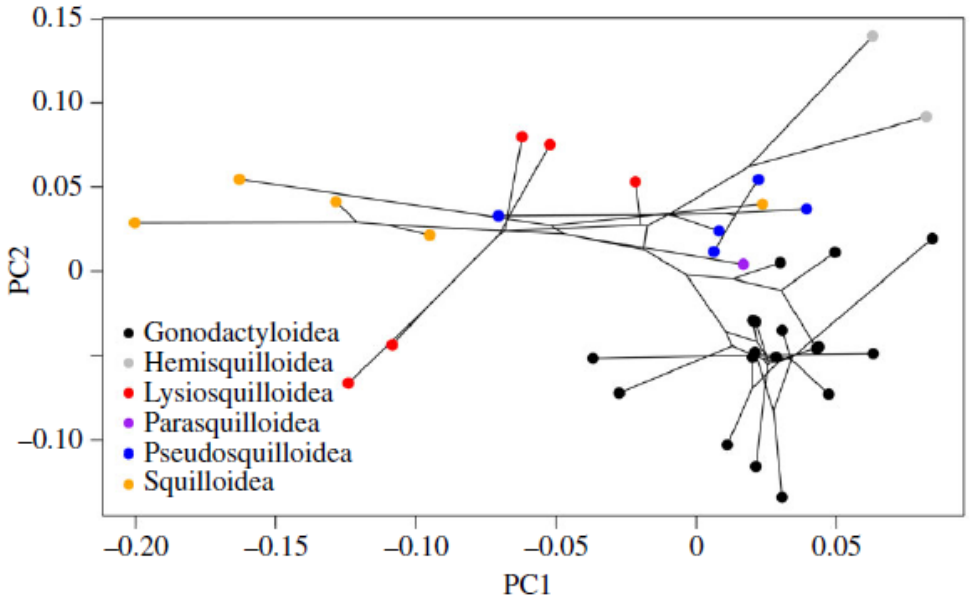

Figure 5. This phylomorphospace of the stomatopod linkage system illustrates the mechanically equivalent nature of kinematic transmission (KT). The morphospace is composed of PC axes 1 and 2 from a landmark-based PC analysis of 36 stomatopod species representing overall morphology of the linkage system. Previous work showed that the four-bar system in spearing clades (Lysiosquilloidea, Parasquilloidea, Pseudosquilloidea and Squilloidea; shown in colour) all evolve towards high KT values. However, this phylomorphospace indicates that each clade does so with distinctive morphologies (sometimes multiple morphologies within clades). Furthermore, certain taxa from the Parasquilloidea and Pseudosquilloidea clades inhabit morphospace adjacent to the smasher clade (Gonodactyloidea; shown in black). (Online version in colour.)

(Anderson & Patek 2015; *Proc. B*)

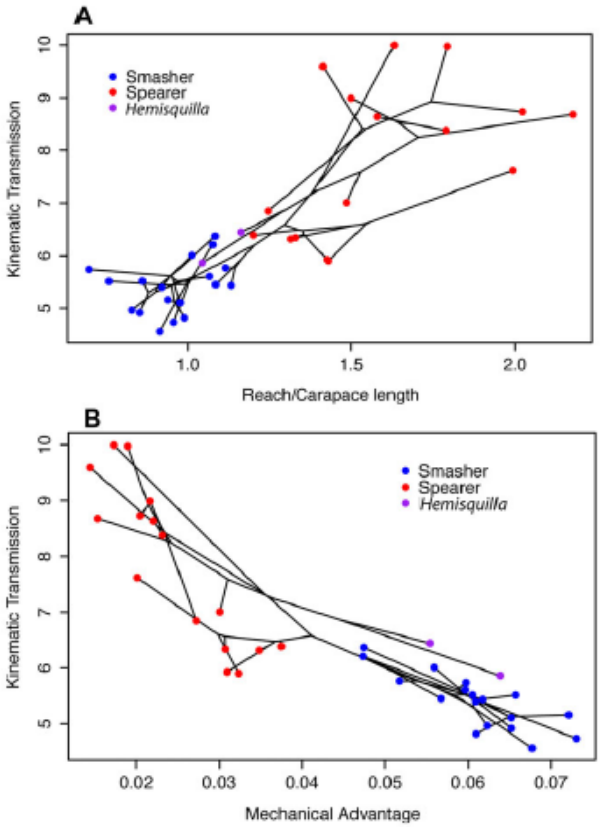

Figure 6. Two phylomorphospaces illustrate the disparate evolutionary variation of our biomechanical metrics overlaid with the stomatopod tree topology. (A) Phylomorphospace of Reach/size versus KT. (B) Phylomorphospace of MA versus KT. Smashers (in blue) represent a monophyletic clade within the stomatopods that trends toward low values of both KT and Reach/size and high values of MA. This combination implies low appendage extension combined with strikes with potentially high force and speed. Spearers (in red) exhibit a wider range of evolutionary variation in KT and Reach/size, yet their lowest values of KT and Reach/size nearly always exceed the highest values in smashers. Spearers also show low values of MA. The two *Hemisquilla* species (in purple) fall at the intersection of smasher and spearers in terms of KT and Reach/size, yet fall within the smasher range for MA. Note that the taxa with the highest values of Reach/size and KT and lowest values of MA are not necessarily all closely related, potentially illustrating multiple invasions of this morphospace by spearing clades.

(Anderson et al. 2014; *Evolution*)

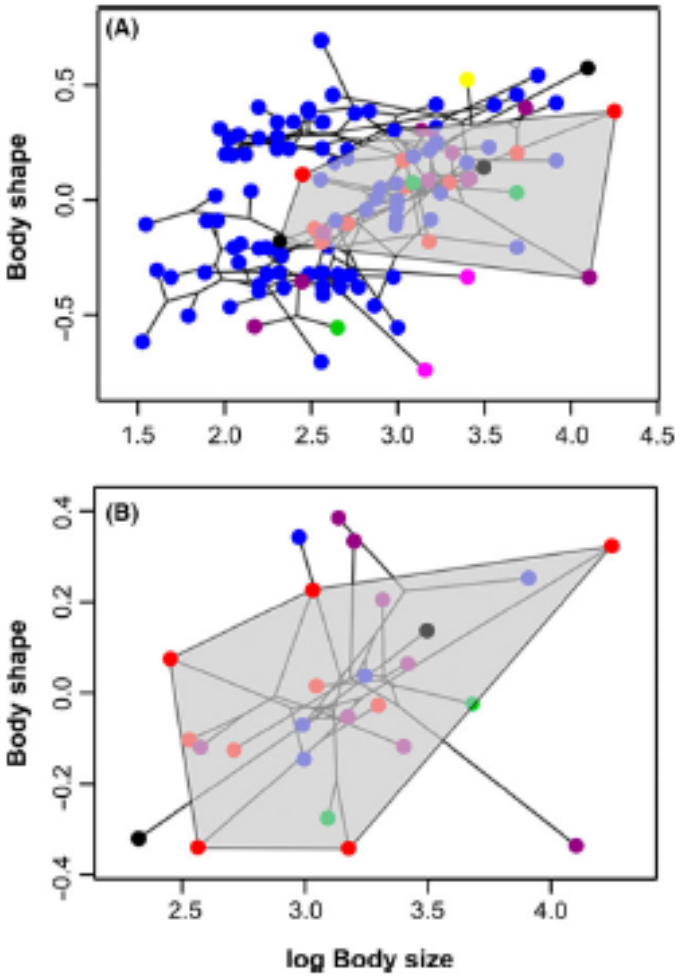

Fig. 6 Phylomorphospace plot for subfamily Hypostominae (A) and genus *Hypostomus* (B). Colours correspond to geographical area classifications used in the ancestral area estimation (Fig. 1). The *y*-axis is the first principal component (PC) from a size-corrected PC analysis of log-normalized linear distances between 31 homologous landmarks distributed across the head, body and fins (following landmarks originally proposed by Armbruster 2003a,b) and the *x*-axis is log maximum body size (MBS). Shaded convex hulls enclose all examined species of *Hypostomus* (A) and all examined species of *Hypostomus* from the Paraná River basin (B).

(Silva et al. 2016; *Mol. Ecol.*)

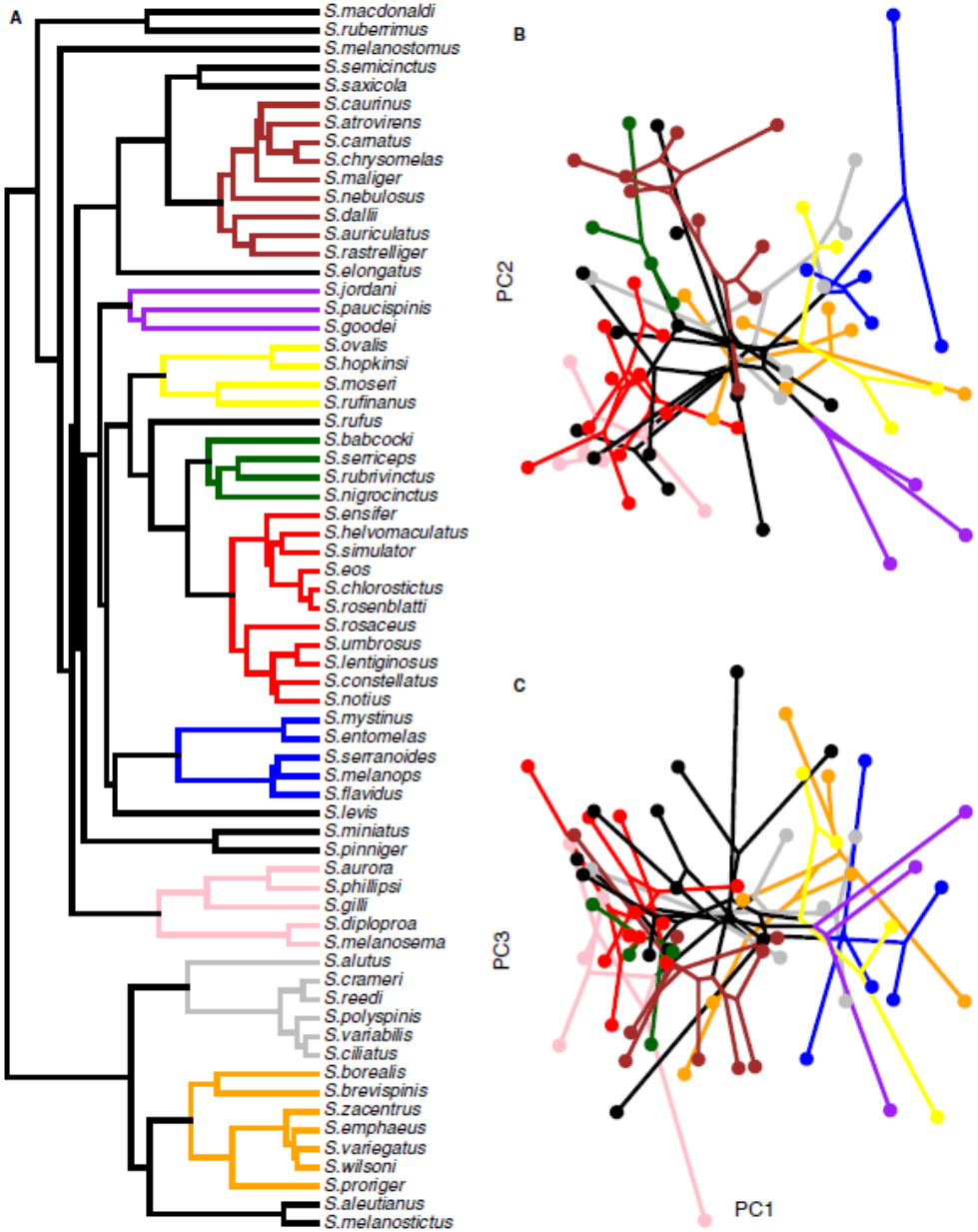

Figure 4. A, phylogenetic tree for 66 species of north-east Pacific rockfish. Notable subclades are highlighted in colour: *Pteropodus* (brown), *Sebastodes* (purple), *Acutomentum* (yellow), *Sebastichthyes* (green); *Sebastomus* (red), *Sebastosomus* (blue), *Eosebastes* (pink), *Sebastes* (grey) and Clades A + B from Hyde and Vetter (2007) (orange). B, phylomorphospace plot projecting the tree into PC shape space (PC1 and PC2), with ancestral characters estimated using maximum likelihood and subclades coloured to match the tree. C, phylomorphospace for PC1 and PC3.

(Ingram 2015; *Biol. J. Linn. Soc.*)

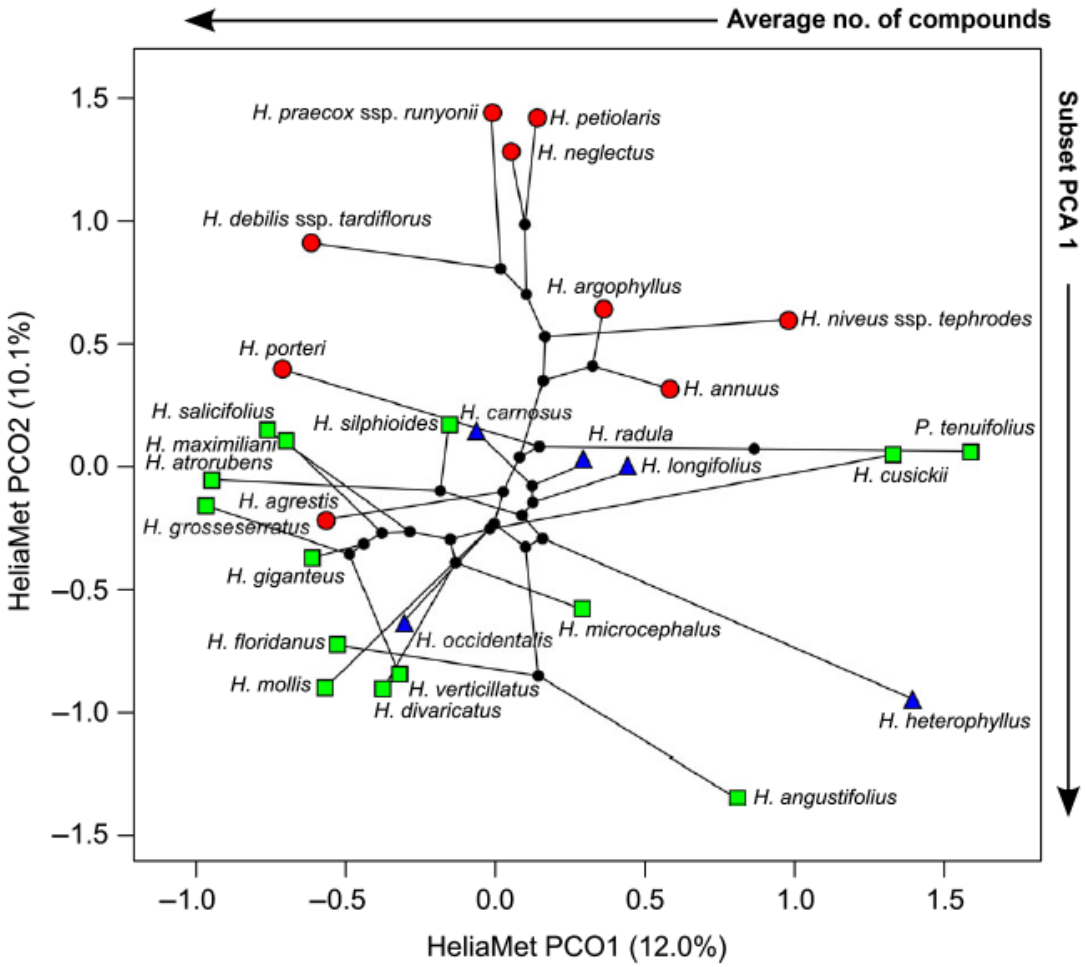

Fig. 3 Evolution of the two primary axes of secondary metabolite composition across *Helianthus*, as defined by species-level principal coordinates analysis and plotted using the *phylomorphospace* function in *phytools* (Revell, 2012). Species are coded by growth form and life history: annuals (red circles), erect perennials (green squares), and basal rosette perennials (blue triangles). Species are connected by phylogenetic relationships, with reconstructed ancestral states of internal nodes plotted in trait space. Note that HeliaMet PCO1 is strongly negatively correlated with the average number of compounds per species ($R^2 = 0.82$; Table 1), HeliaMet PCO2 is strongly negatively correlated with abundance of the most common compounds as described by HeliaMet subset PC1 ($R^2 = 0.56$; Table 1), and HeliaMet PCO2 is significantly associated with life history by PGLS-ANOVA ($P = 0.0185$), with annuals significantly different from both types of perennials by post hoc test.

(Mason et al. 2015; *New Phytol.*.)

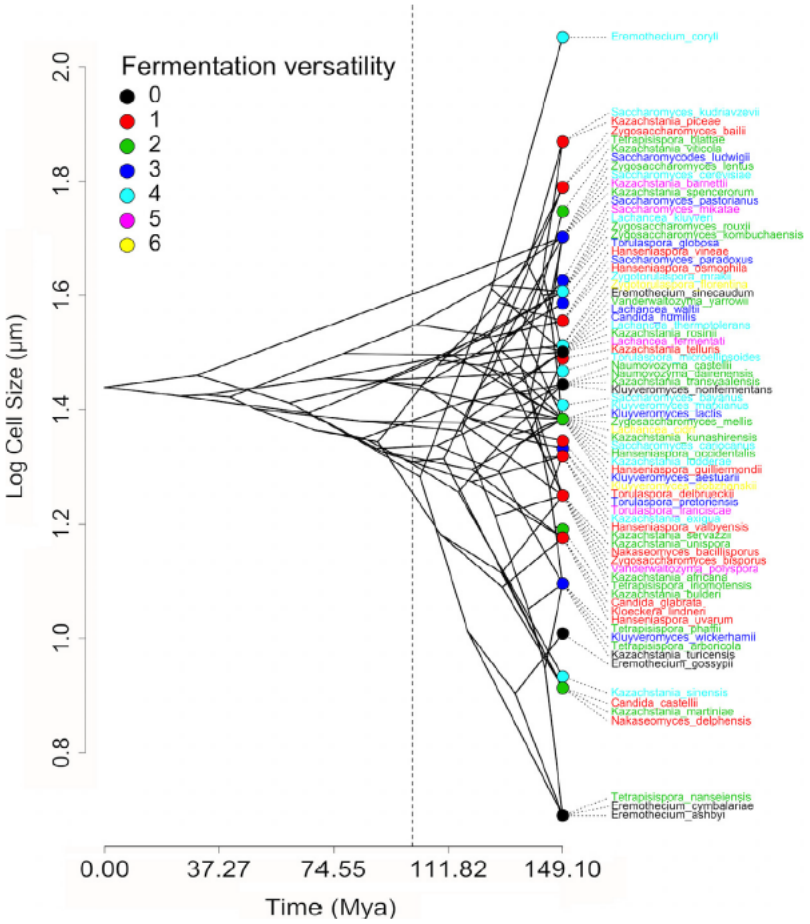

Figure 2. Phenogram showing the diversification of cell-size across time, in our working phylogeny. The dotted line indicates, approximately, the Whole Genome Duplication that occurred 100 MYA (see the text for details).

(Paleo-Lopez et al. 2016; *Ecol. Evol.*)

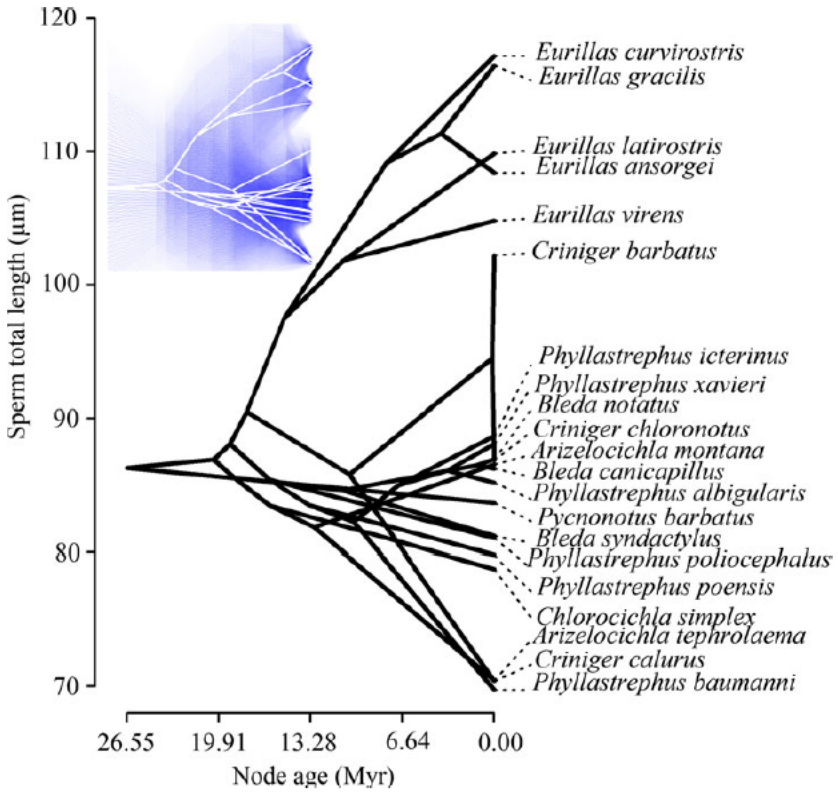

Figure 3. Traitgram showing the projection of the greenbul phylogeny into a space defined by sperm total length (µm) (*y*-axis) and node age [i.e. time since divergence from the root (*x*-axis]. The vertical position of nodes and branches are computed via ancestral character estimation using maximum likelihood. The embedded images indictates uncertainty through increasing transparency of the plotted blue lines around the point estimates, with the entire range showing the 95% confidence interval.

(Omotorigun et al. 2016; *Biol. J. Linn. Soc.*)

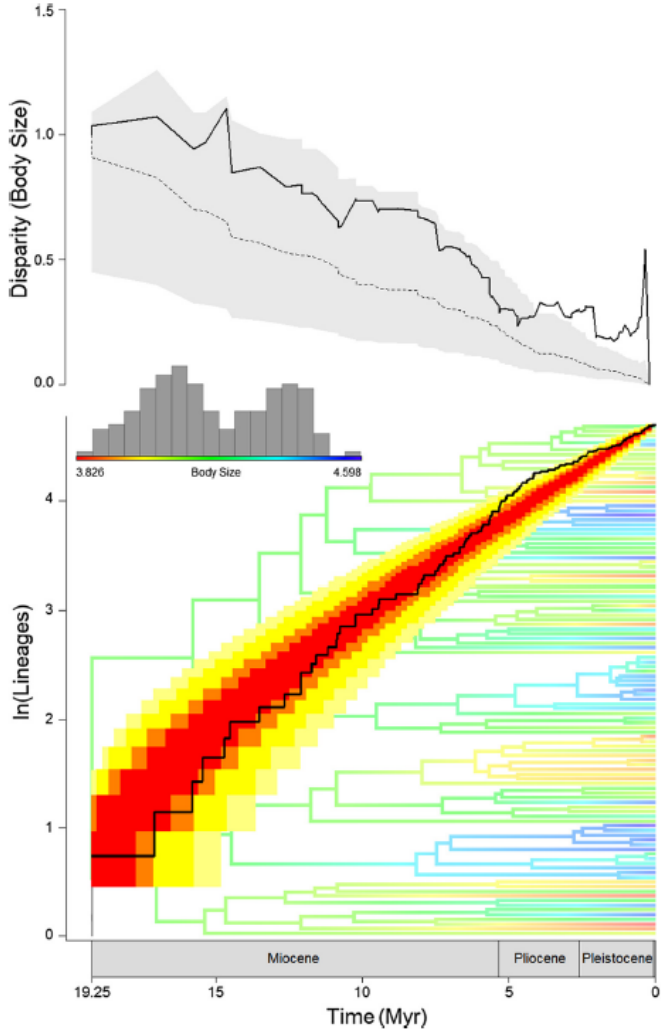

Fig. 2 Tempo and mode of macroevolutionary diversification in *Liolaemus* lizards. The bottom plot shows the lineage through time (LTT) curve of species accumulation over time (solid line) and the 95 % (yellow area) to 50 % (red area) confidence intervals (note the most recent pulse is borderline). The phylogenetic tree in the background shows a maximum-likelihood phylogenetic reconstruction of ancestral body sizes (ln-transformed) along the branches and nodes of the tree, and the interspecific range is shown in the coloured bar with the frequency distribution of SVL of the entire genus. The top plot shows mean subclade disparity through time (DTT) for body size (solid line), compared with the median subclade DTT (calculated based on 10,000 simulations) of phenotypic evolution on the genus phylogeny under a Brownian motion model (dashed line). The grey shaded area represents the 95 % confidence interval of DTT range based on simulations of body size disparity

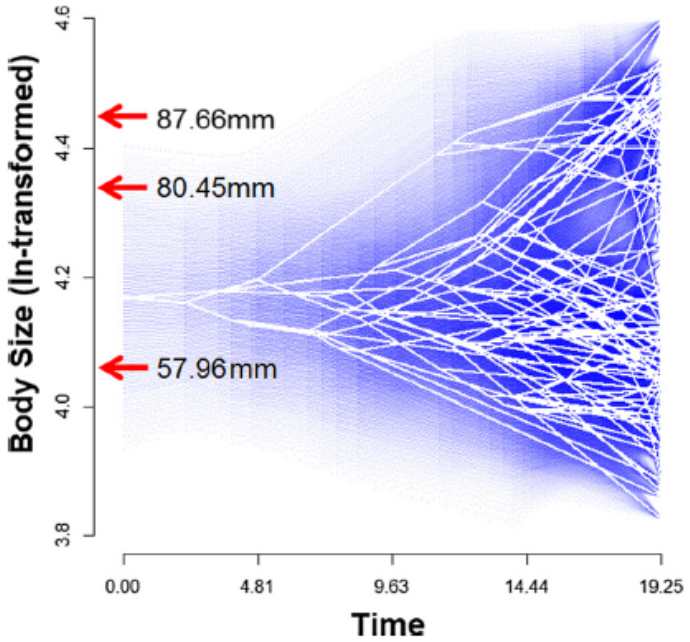

Fig. 3 Projection of the *Liolaemus* phylogeny into a morphospace defined by body size (ln-transformed, on *y*) and time since the clade's origin (on *x*, in My elapsed since the root). Ancestral body size states are estimated using likelihood. The degree of uncertainty is indicated by increasing transparency of the plotted blue lines around the point estimates with the entire range showing the 95 % confidence interval. Red arrows indicate the position of the three body size peaks (in mm) identified by the surface analysis (see text for details)

(Pincheira-Donoso et al. 2015; *BMC Evol. Biol.*)

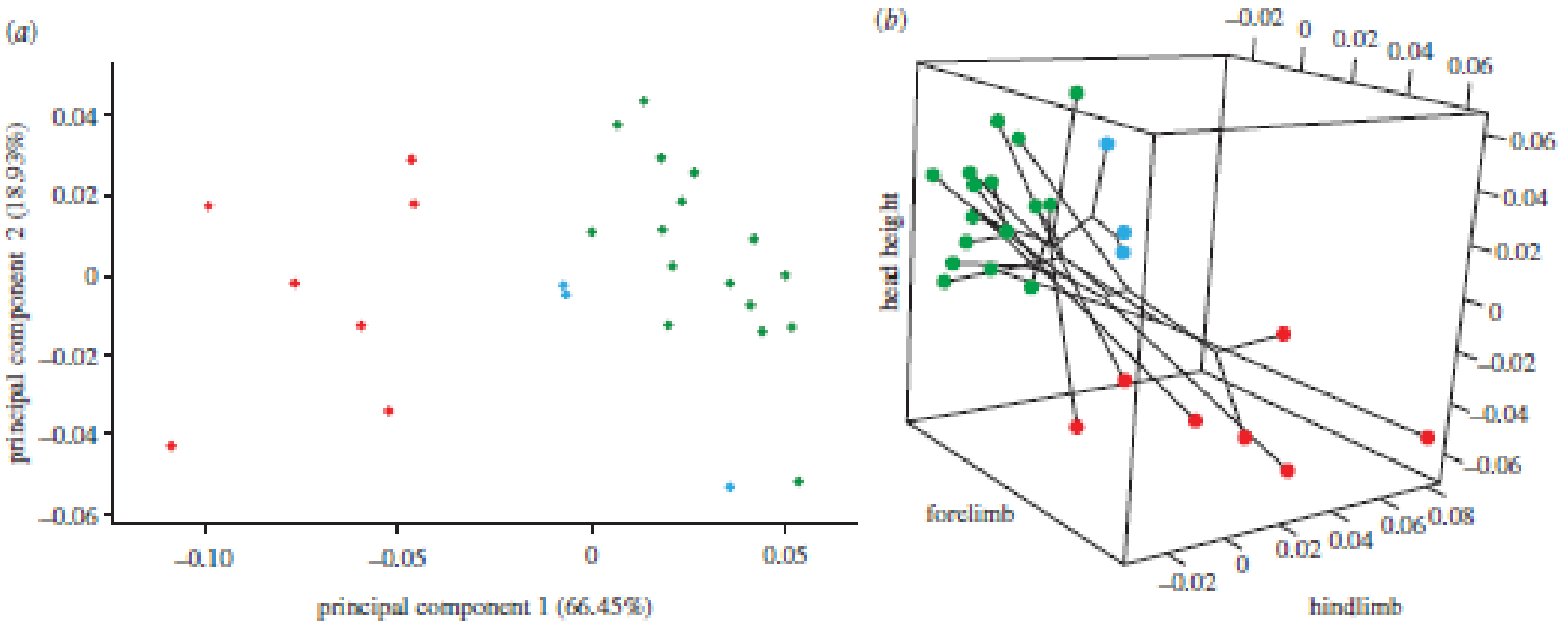

Figure 2. pPCA and three-dimensional phylomorphospace plot. (*a*) Morphological variation among species along pPC1 and pPC2, where each dot represents a species and is coloured by that species' habitat type (figure 1). PC1 separates the rock specialists from the other habitat specialists. (*b*) Size-corrected residual scores from phylogenetic regression are plotted for each of the traits that were identified as different between habitats. Colours correspond to the habitat type for each respective species (figure 1) and the phylogeny is mapped onto morphospace. Regardless of phylogenetic association, species are more closely clustered in morphospace by habitat.

(Blom et al. 2016; *Proc. B*)

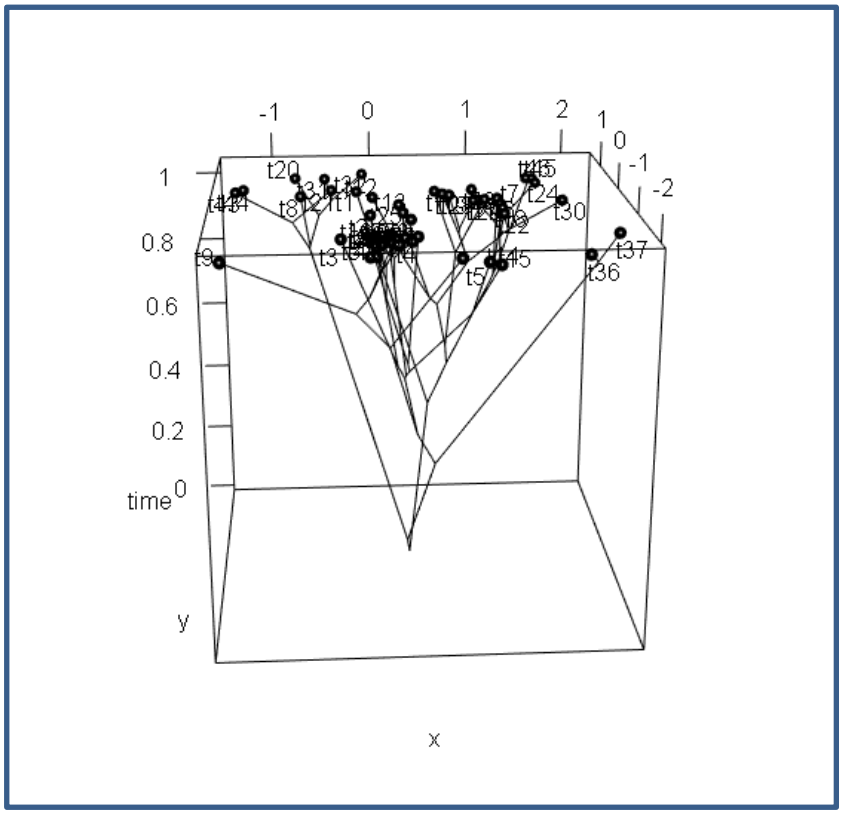

Figure. Example 3D traitgram.

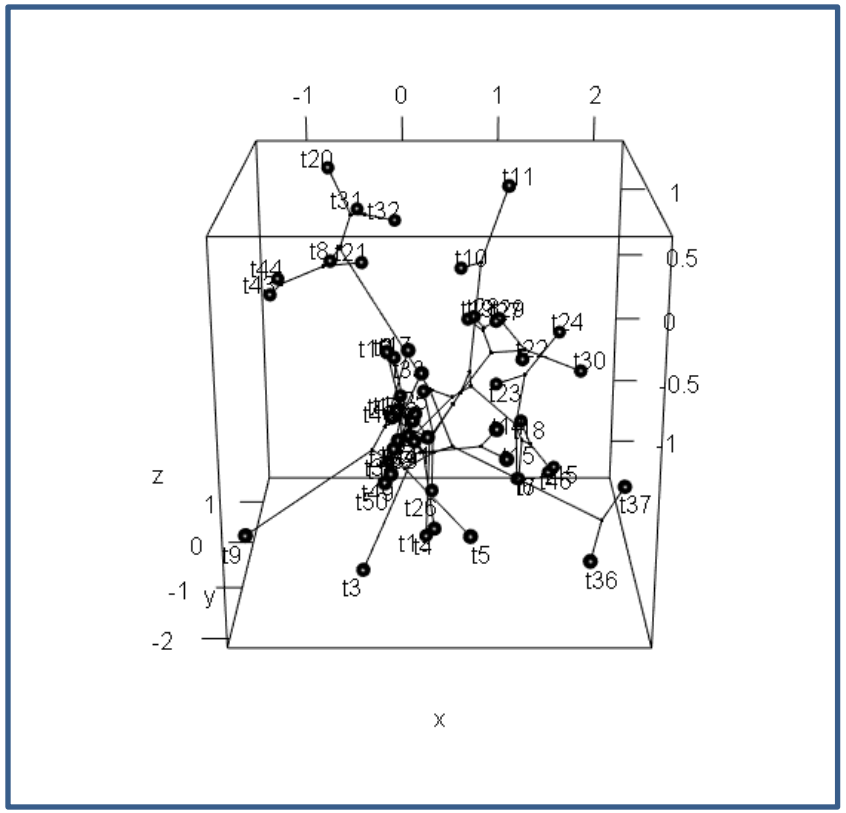

Figure. Example 3D phylomorphospace.

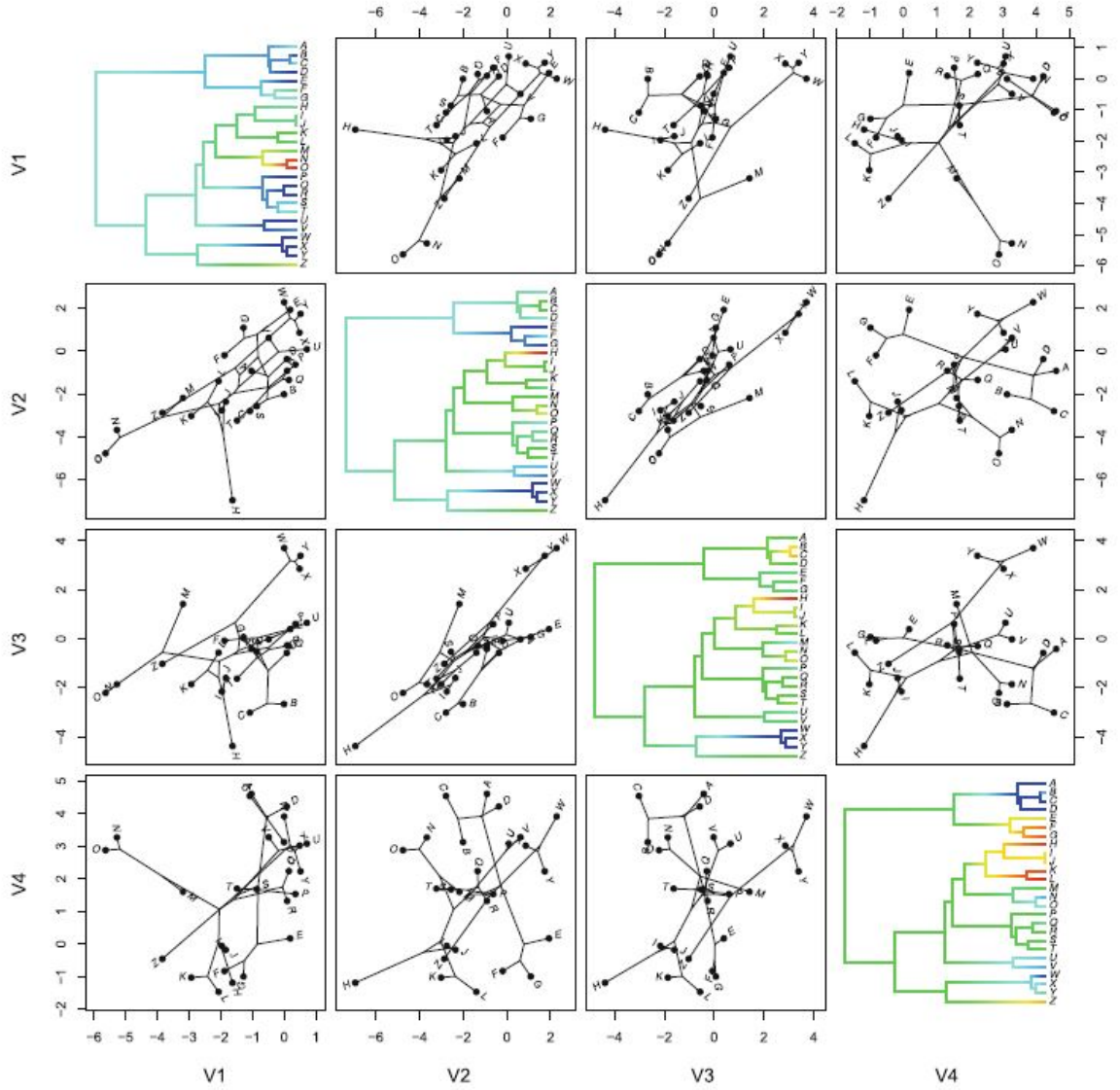

Fig. 4.9 Simulated four-trait phylogenetic scatterplot matrix. Each diagonal element is a continuous character projection on the tree in which red branches indicate small values for the phenotypic trait and blue branches large values, whereas off-diagonals are phylomorphospaces for each *i*, *j*th pair of traits

Biogeographic methods

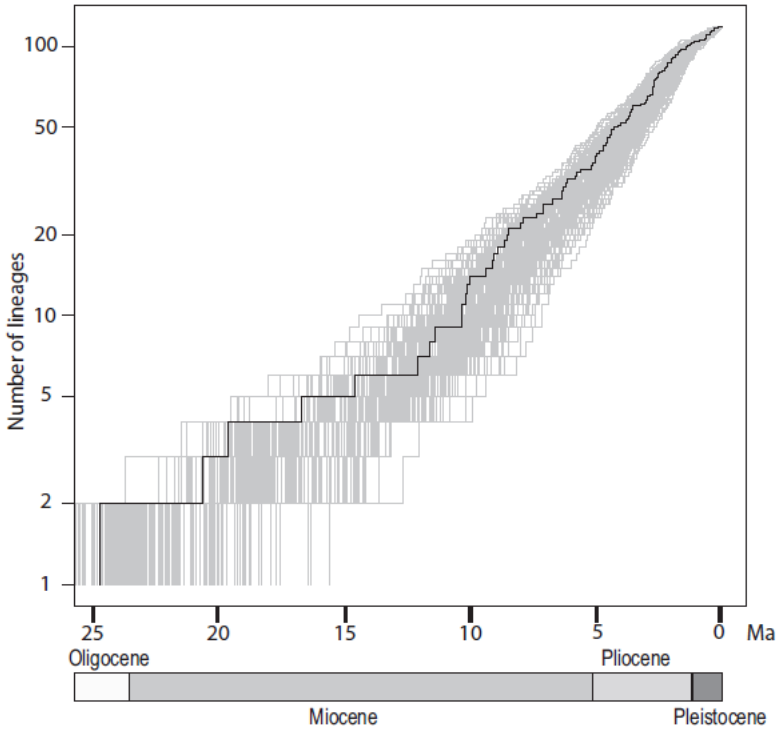

Figure 3 Lineages-through-time plot of the African danthonioids, showing no change in diversification rate. The black curve represents the maximum clade credibility tree, and grey curves represent 200 trees randomly sampled from the posterior distribution from the set of BEAST trees.

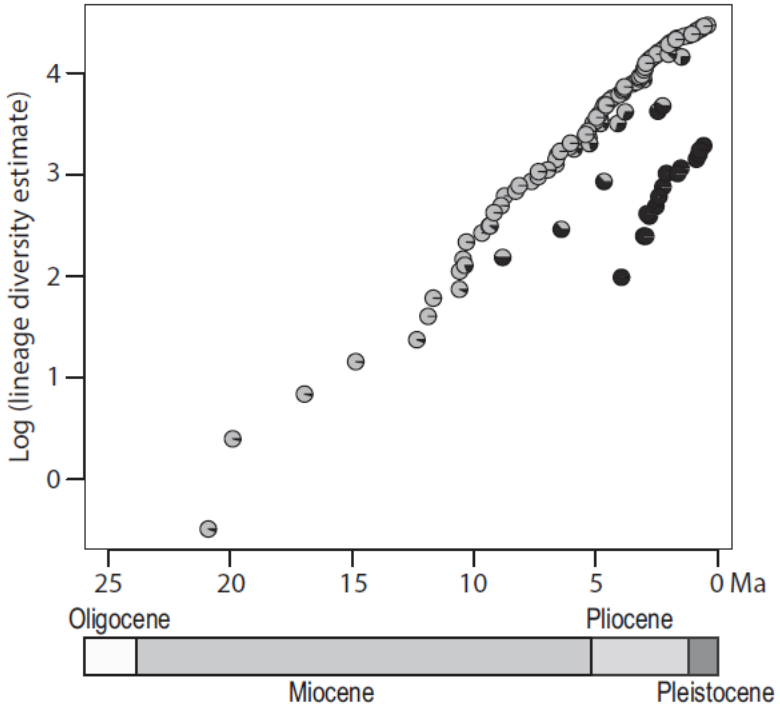

Figure 4 The comparison between the accumulation of diversity in winter rainfall (WR) and summer rainfall (SR) lineages of the African danthonioids. Each point reflects a node on the maximum clade credibility tree from the BEAST analysis, the diversity estimate is the marginal probabilities of WR and SR multiplied by the summed probabilities of WR and SR of all ancestral nodes, with light grey indicating WR and dark grey SR.

(Linder & Bouchenak-Khelladi 2015; *J. Biogeogr.*)

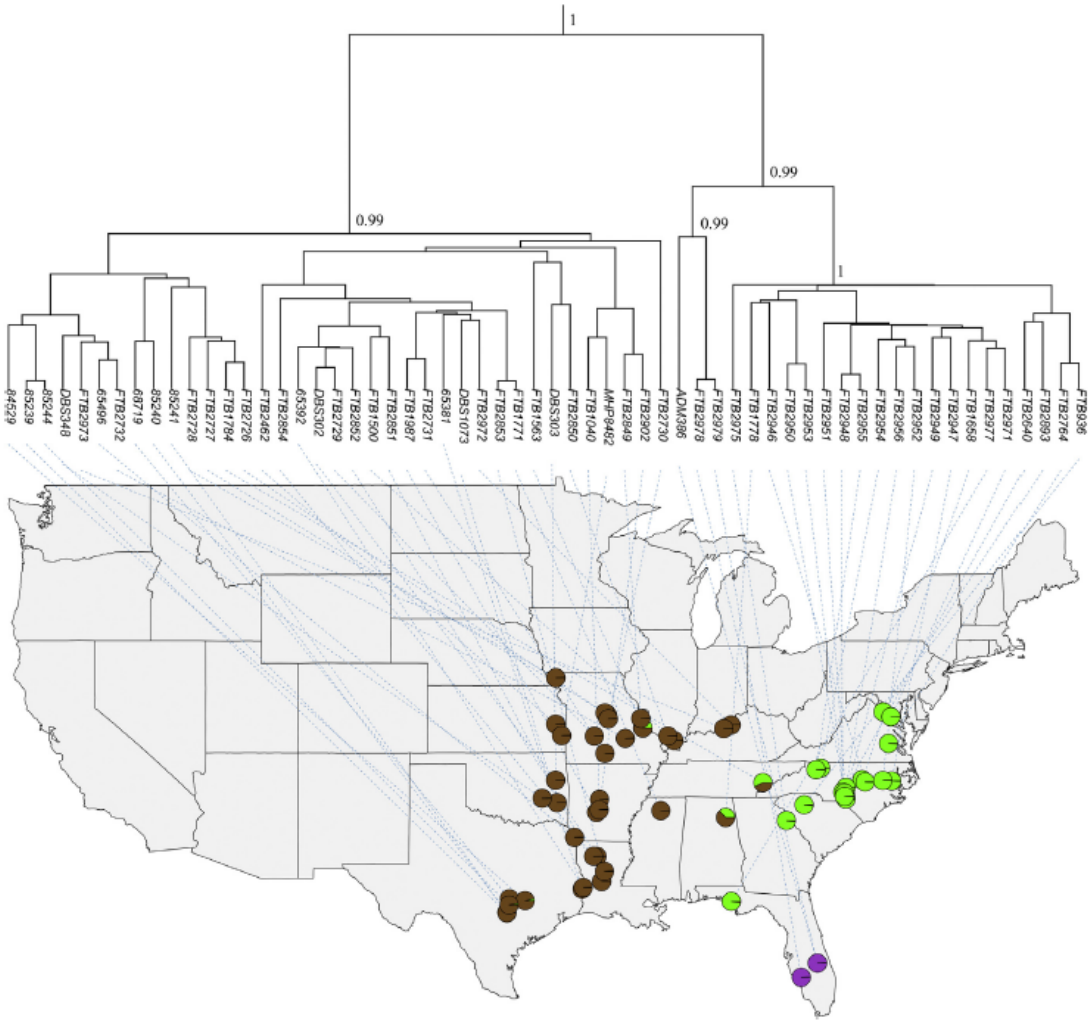

Fig. 2. Admixture map and phylogeographic relationships among taxa. Individual gene trees are reported in Supplementary Material 1.

(McKelvy & Burbrink 2017; *MPE*)

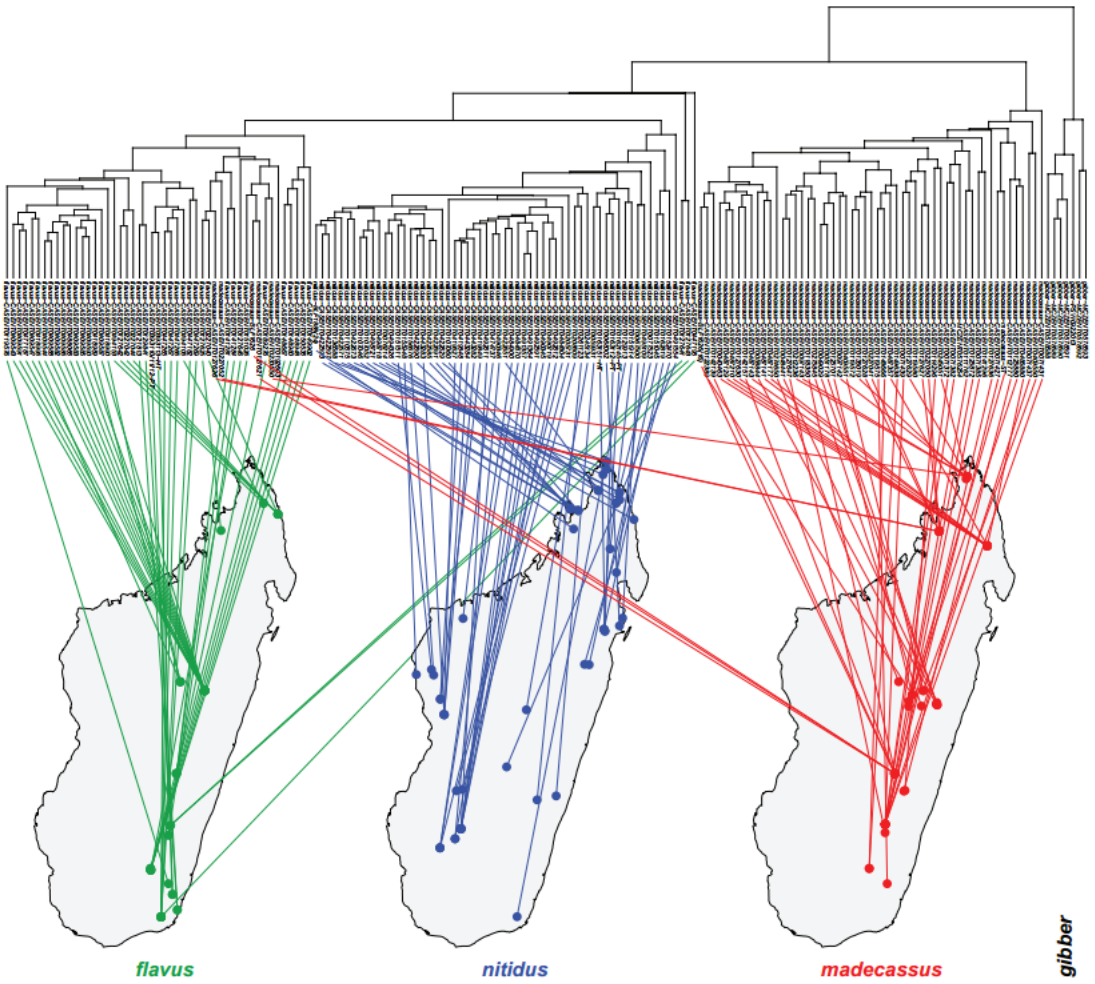

Figure 2. Dendrogram to geographic map. Dendrogram solution is linked on the map of Madagascar. Color codes for species are as follows: *Nesomyrmex flavus* sp. n.: green, *N. gibber*: black, *N. madecassus*: red, *N. nitidus* sp. n.: blue. Samples of *N. gibber* found in Mauritius, East to Madagascar (not shown).

(Csősz & Fisher, 2016; *ZooKeys*)

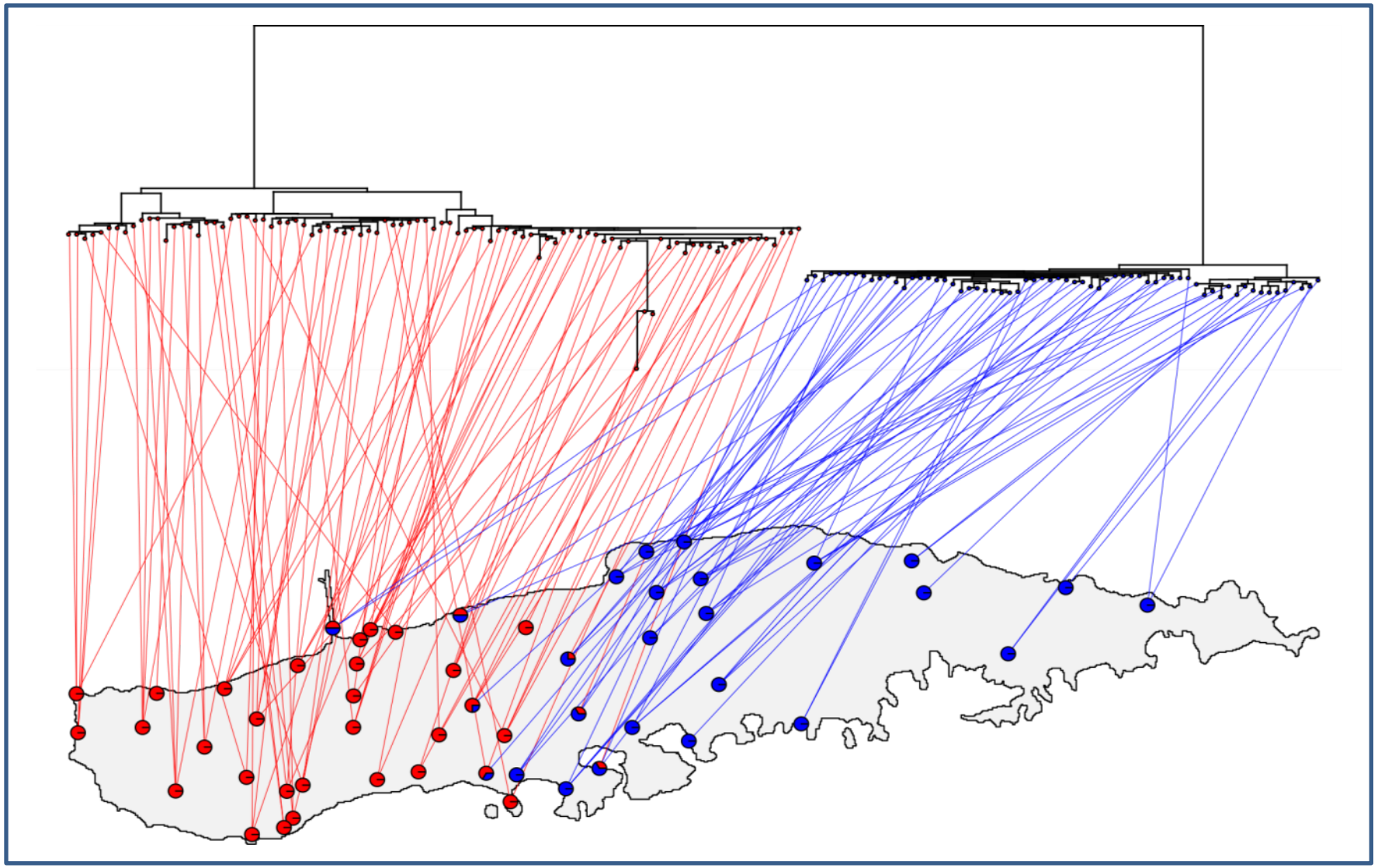

(Quach et al. *In prep*)

New methods

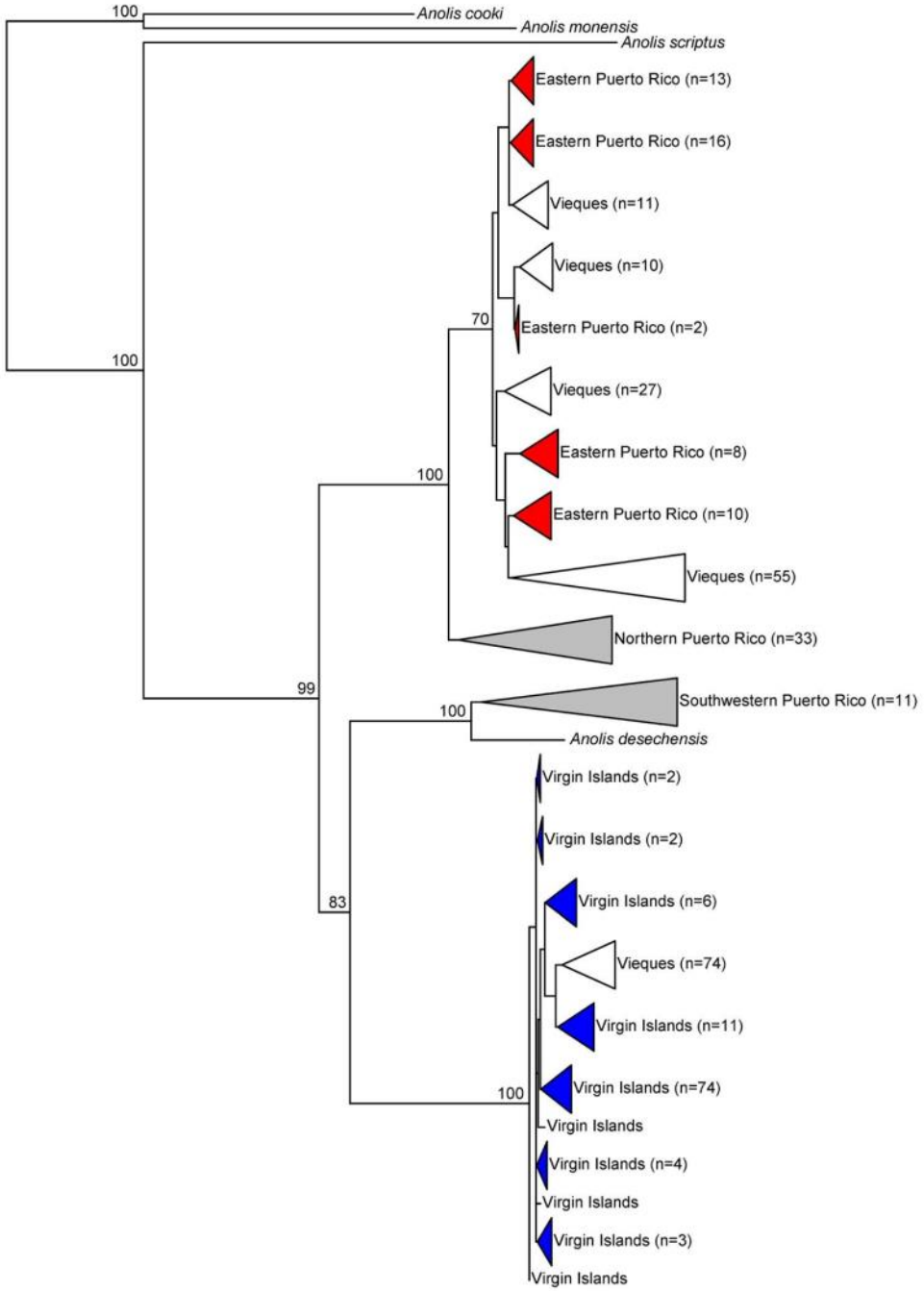

(Quach et al. *In prep*)

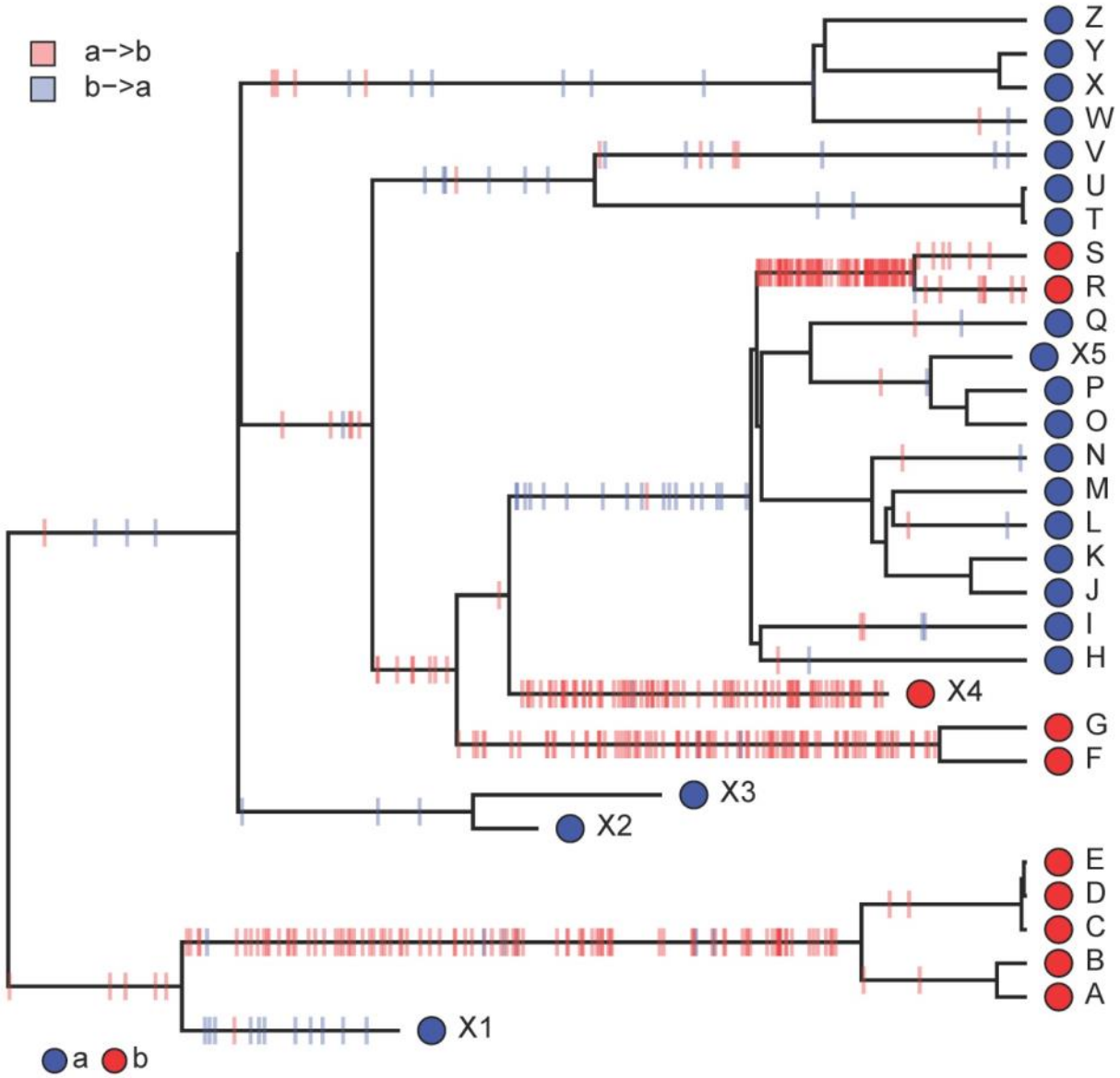

Figure. Posterior distribution of *changes* from stochastic mapping plotted on the tree.

a.

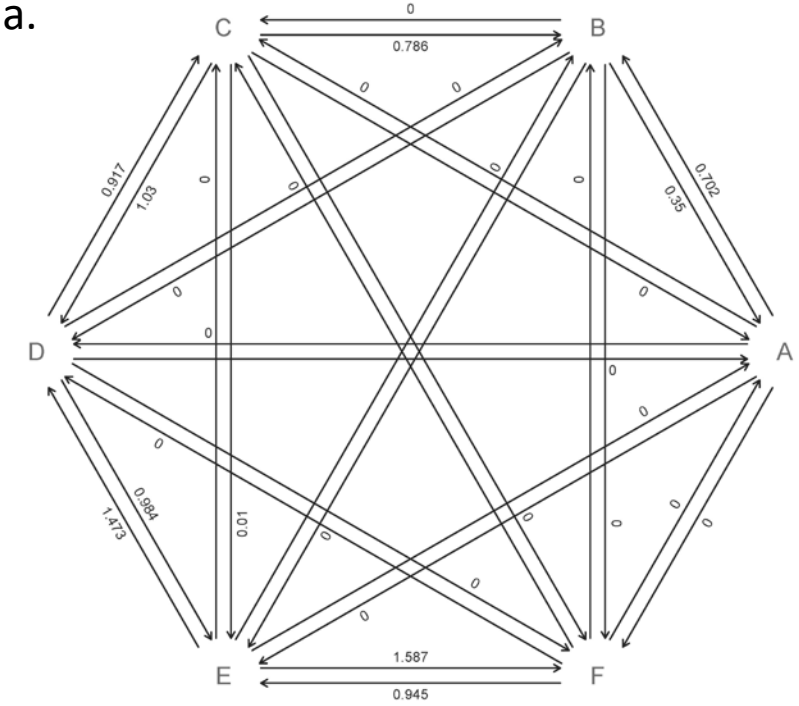

b.

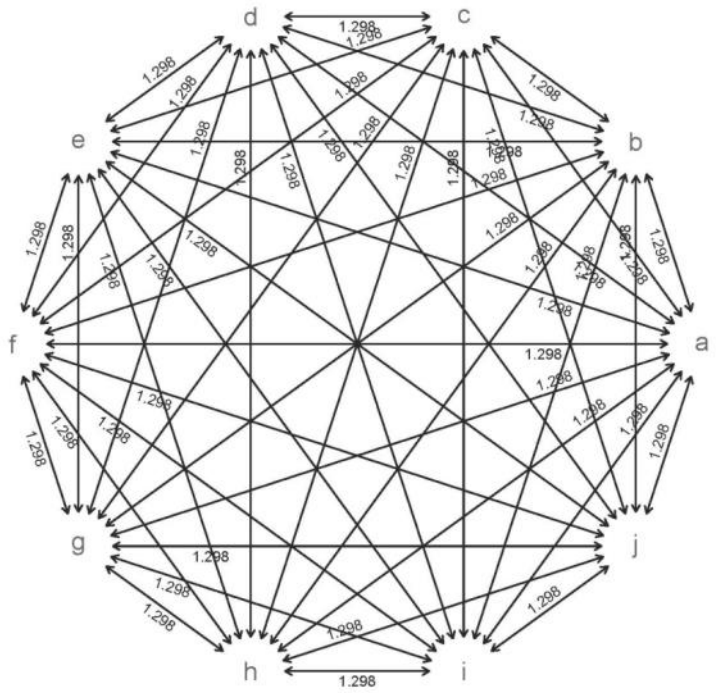

Figure. Example fitted models from (a.) 6 and (b.) 10 state discrete character data on phylogenies.

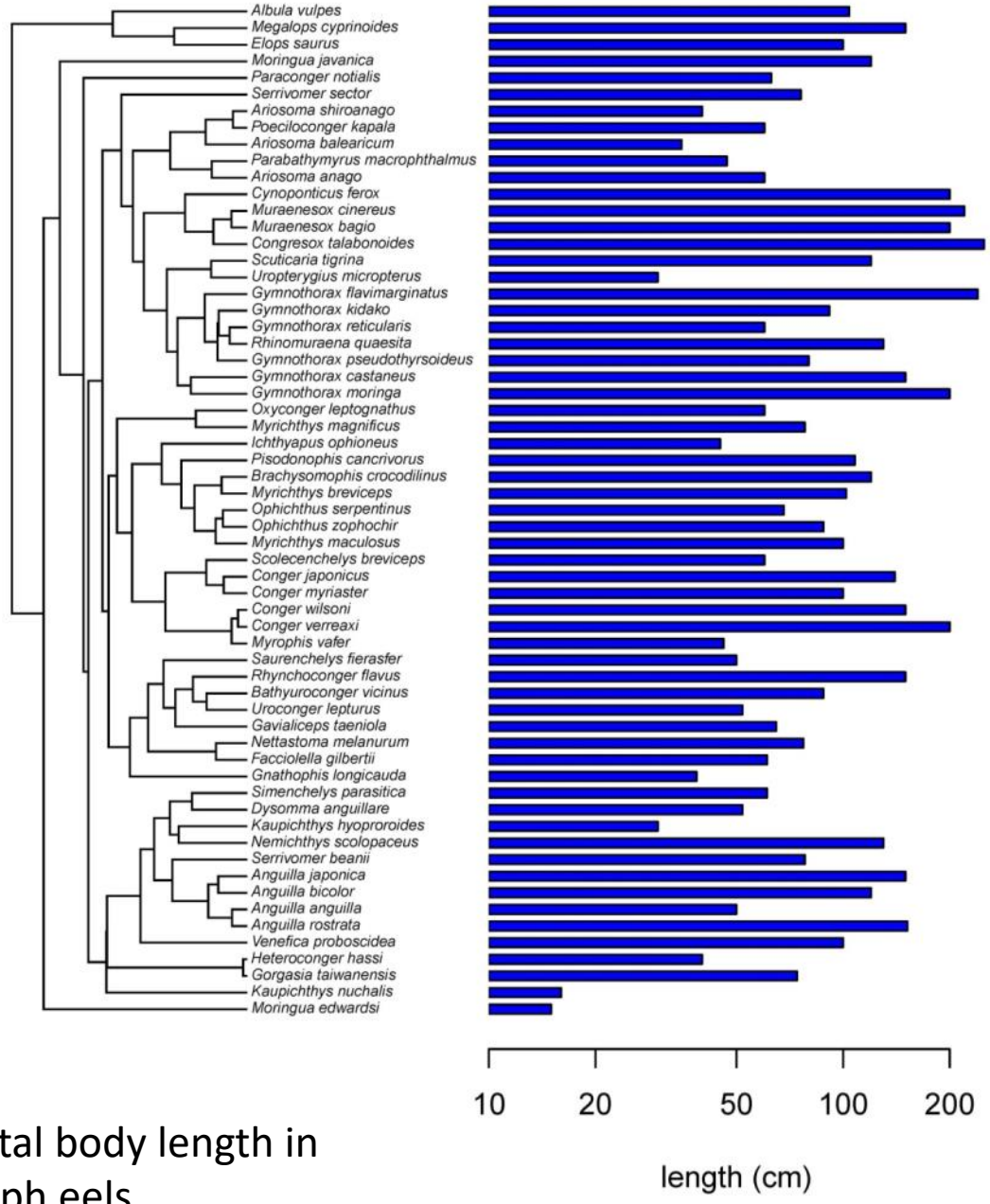

Figure. Total body length in elopomorph eels.

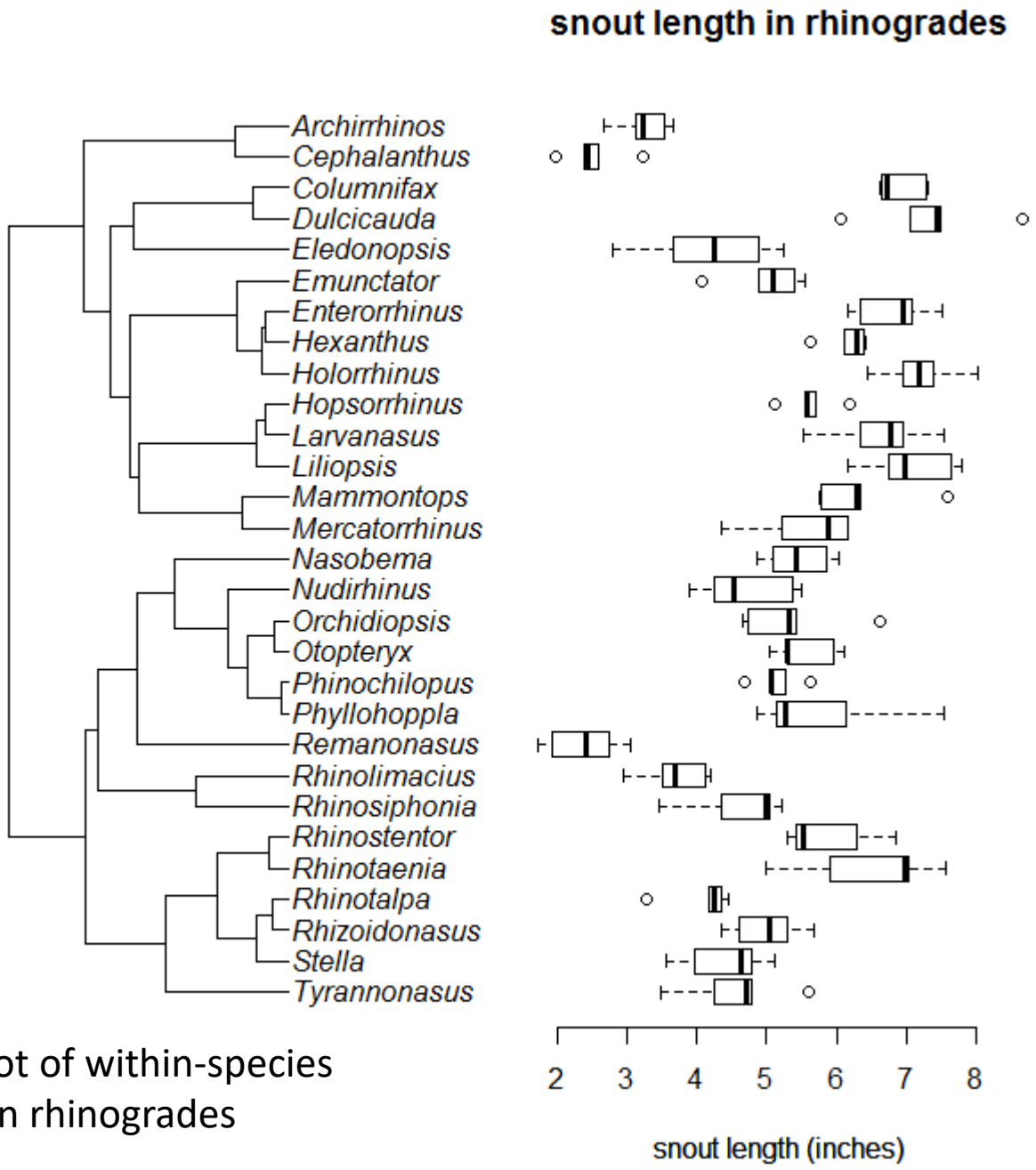

Figure. Phylogenetic boxplot of within-species variability in snout length in rhinogrades (actually, simulated data).

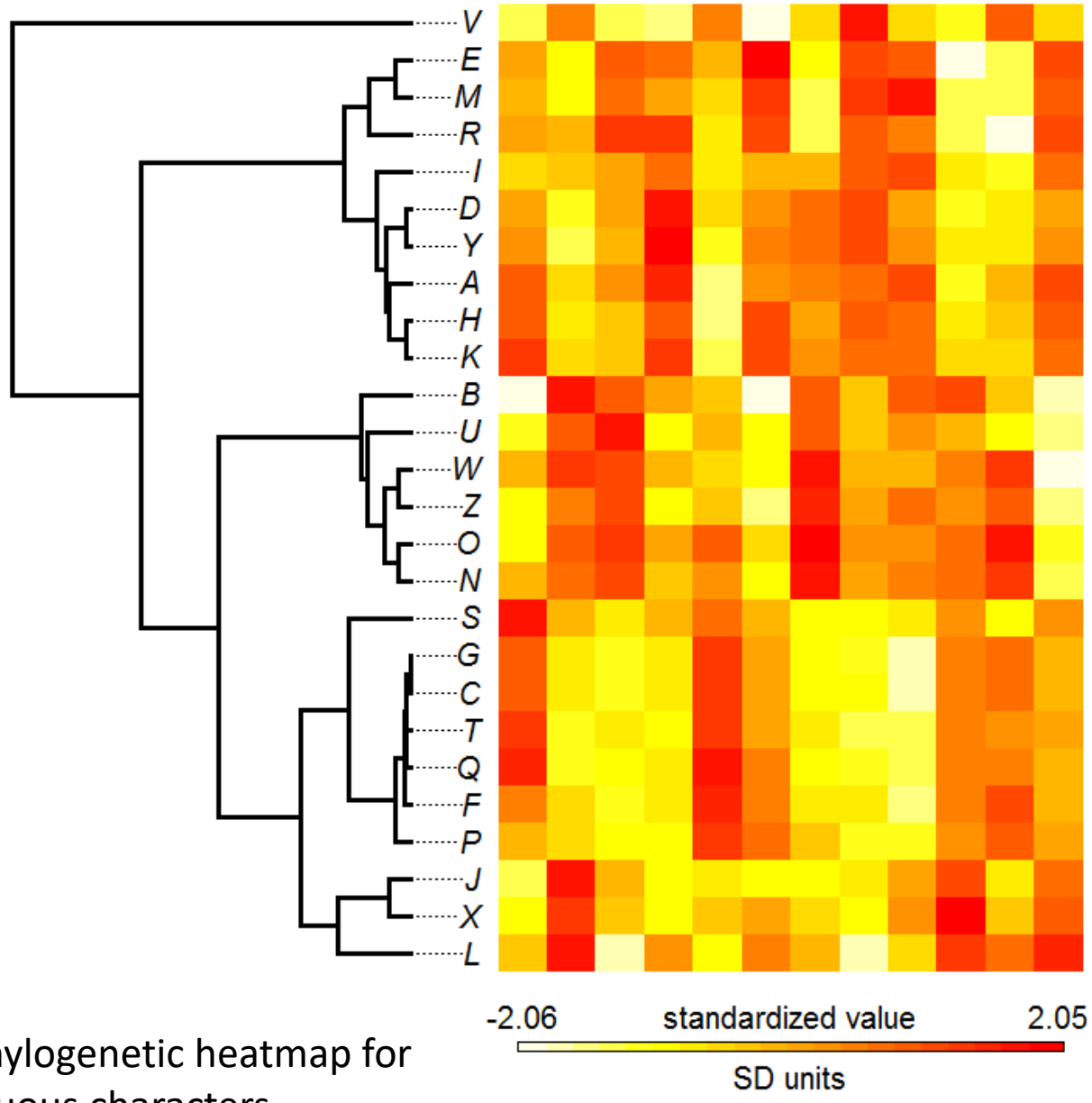

Figure. Phylogenetic heatmap for 10 continuous characters.

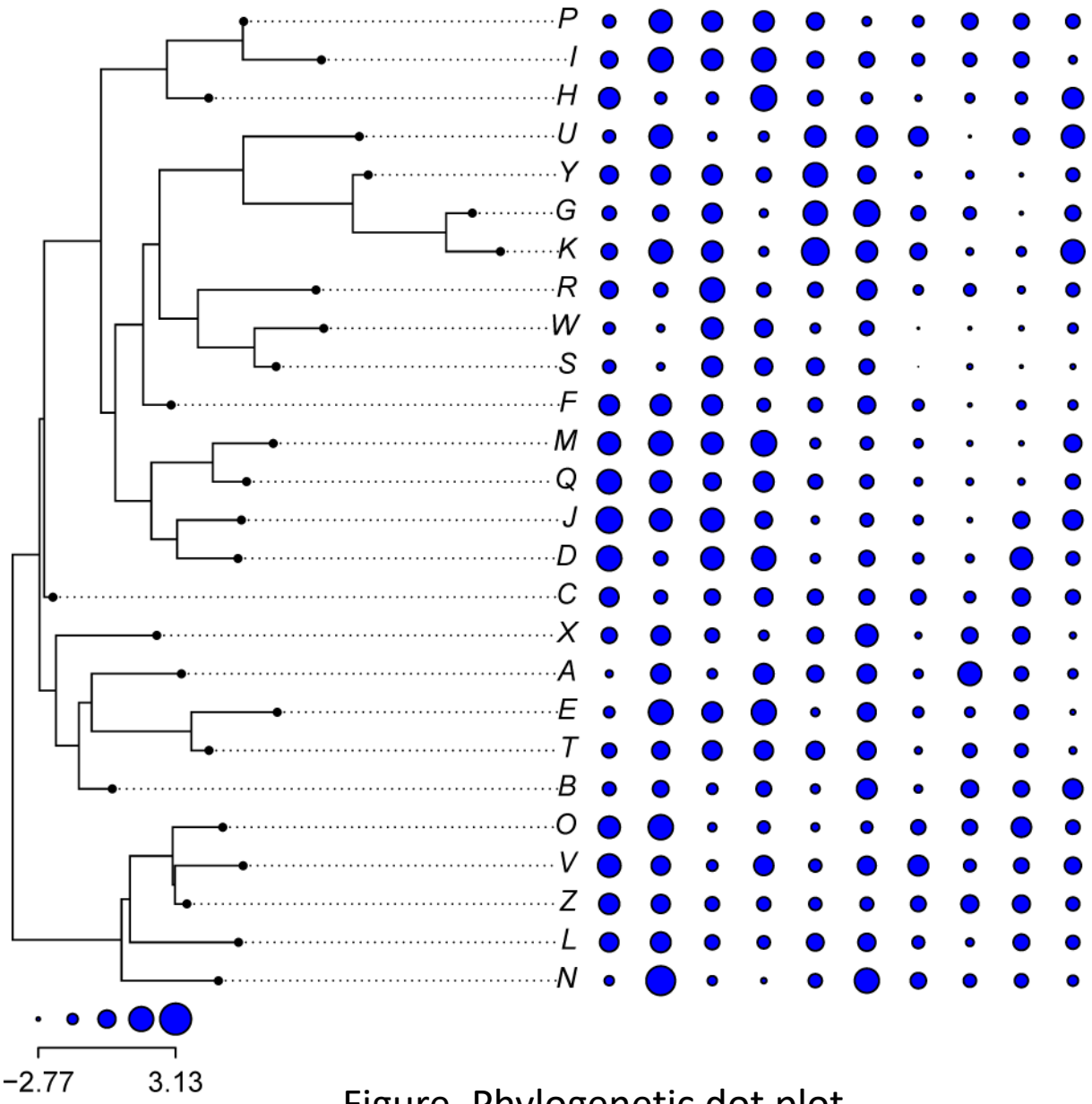

Figure. Phylogenetic dot plot.

Co-phylogenetic plotting

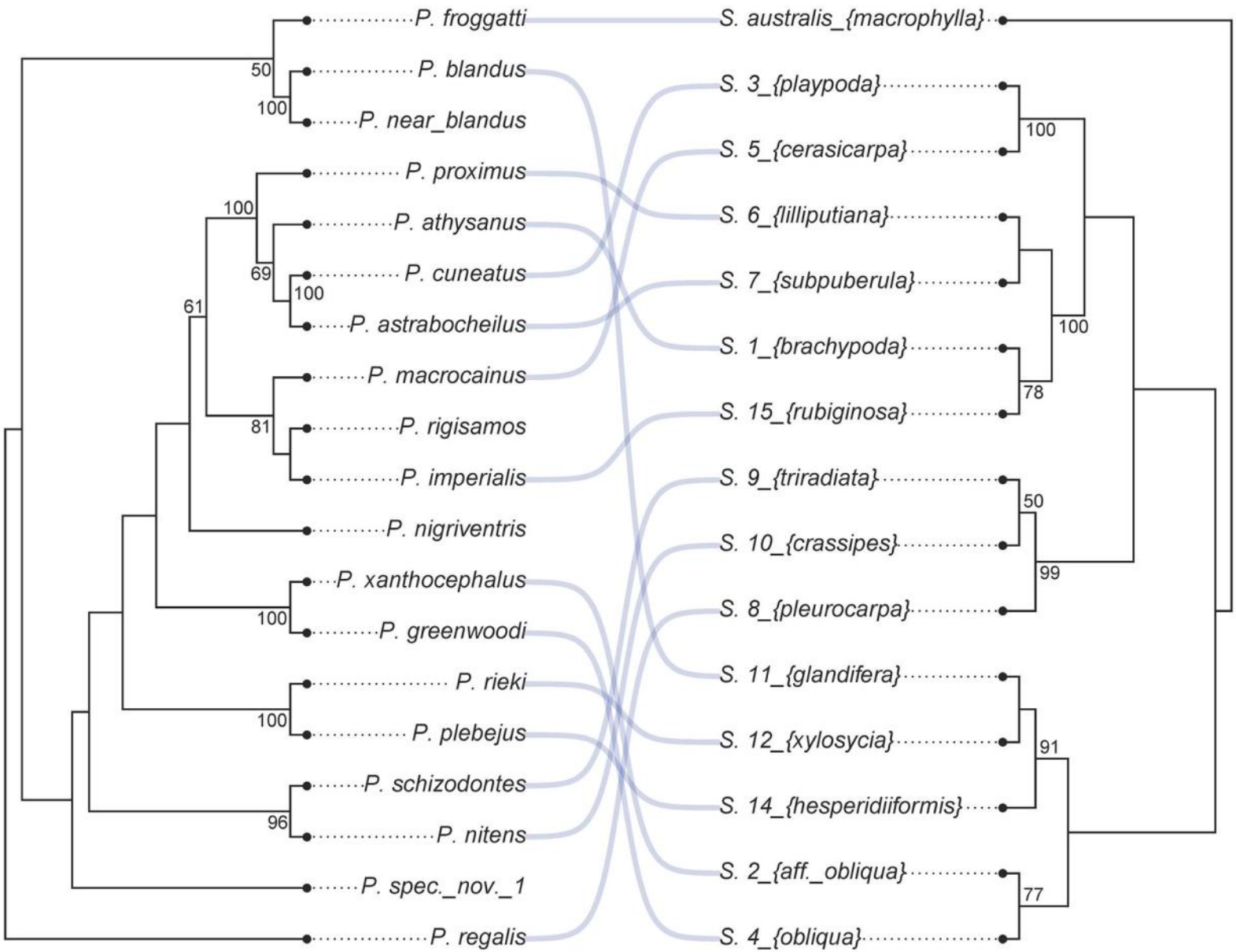

(Lopez-Vaamonde et al. 2001; *MPE*)

$N_1 = N_2 =$	N possible cophylo rotations	Memory to store comparison between rotations
2	4	32 bytes
3	16	64 bytes
4	64	512 bytes
5	256	2 KB
6	1,024	8 KB
7	4,096	32 KB
8	16,384	131 KB
9	65,536	524 KB
10	262,144	2.1 MB
11	1,048,576	8.4 MB
12	4,194,304	34 MB
13	16,777,216	134 MB
14	67,108,864	537 MB
15	268,435,456	2.1 GB
16	1,073,741,824	8.6 GB
17	4,294,967,296	34 GB
18	17,179,869,184	137 GB
19	68,719,476,736	550 GB
20	274,877,906,944	2.2 TB

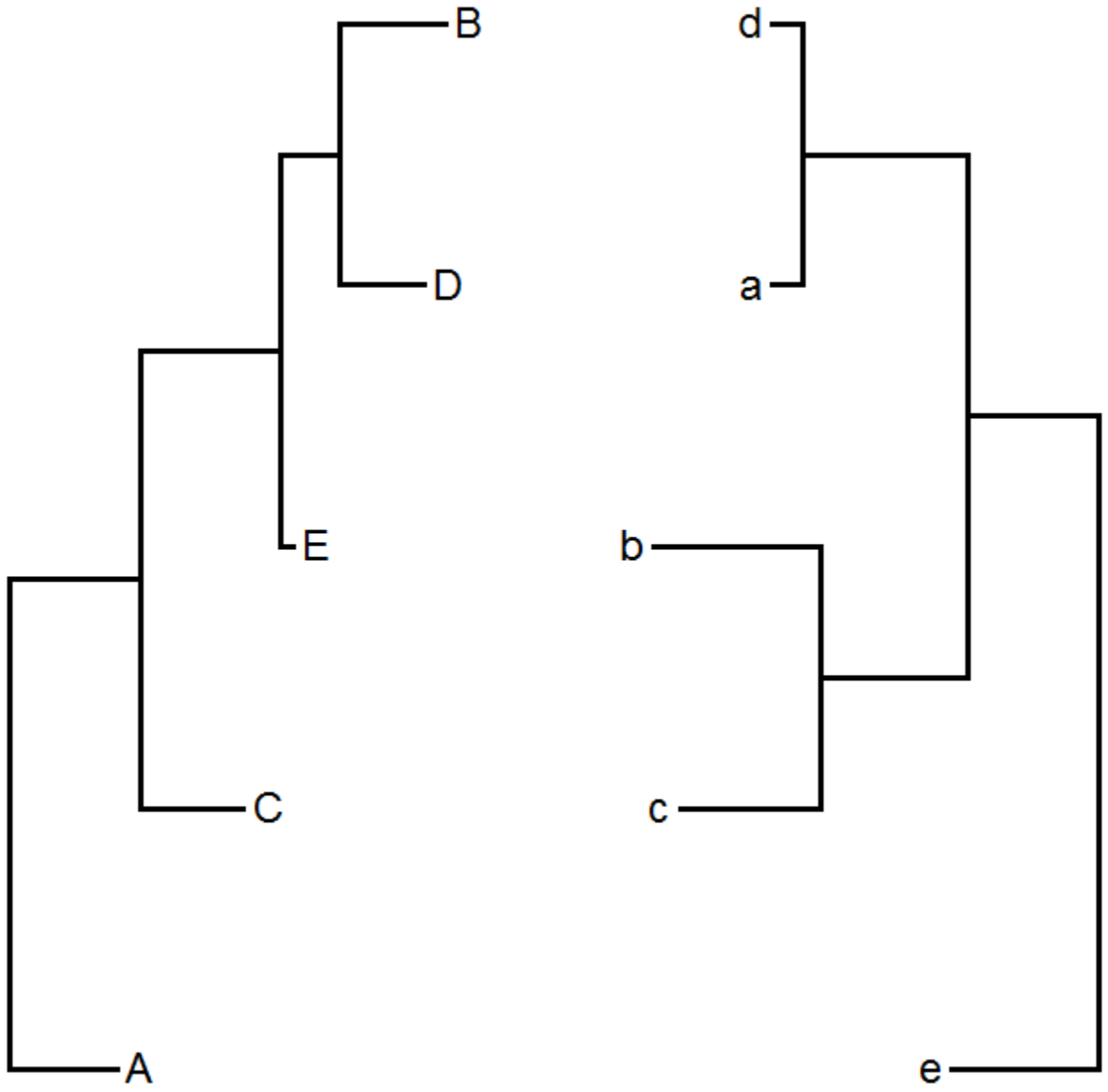
B
D
E
C
A
d
a
b
c
e

Co-phylogenetic plotting

- I have developed a ‘greedy’ optimization routine to find the best tip-matching.
- It involves multiple pre-order tree traversals & we are showing that it is guaranteed to find the best match when co-speciation is perfect (that is, the trees match in their topology).

Co-phylogenetic plotting

- I have developed a ‘greedy’ optimization routine to find the best tip-matching.
- It involves multiple pre-order tree traversals & we are showing that it is guaranteed to find the best match when co-speciation is perfect (that is, the trees match in their topology).
- This is true when some taxa are missing from one tree or the other, or when a clade of one tree matches with a single lineage in the other.

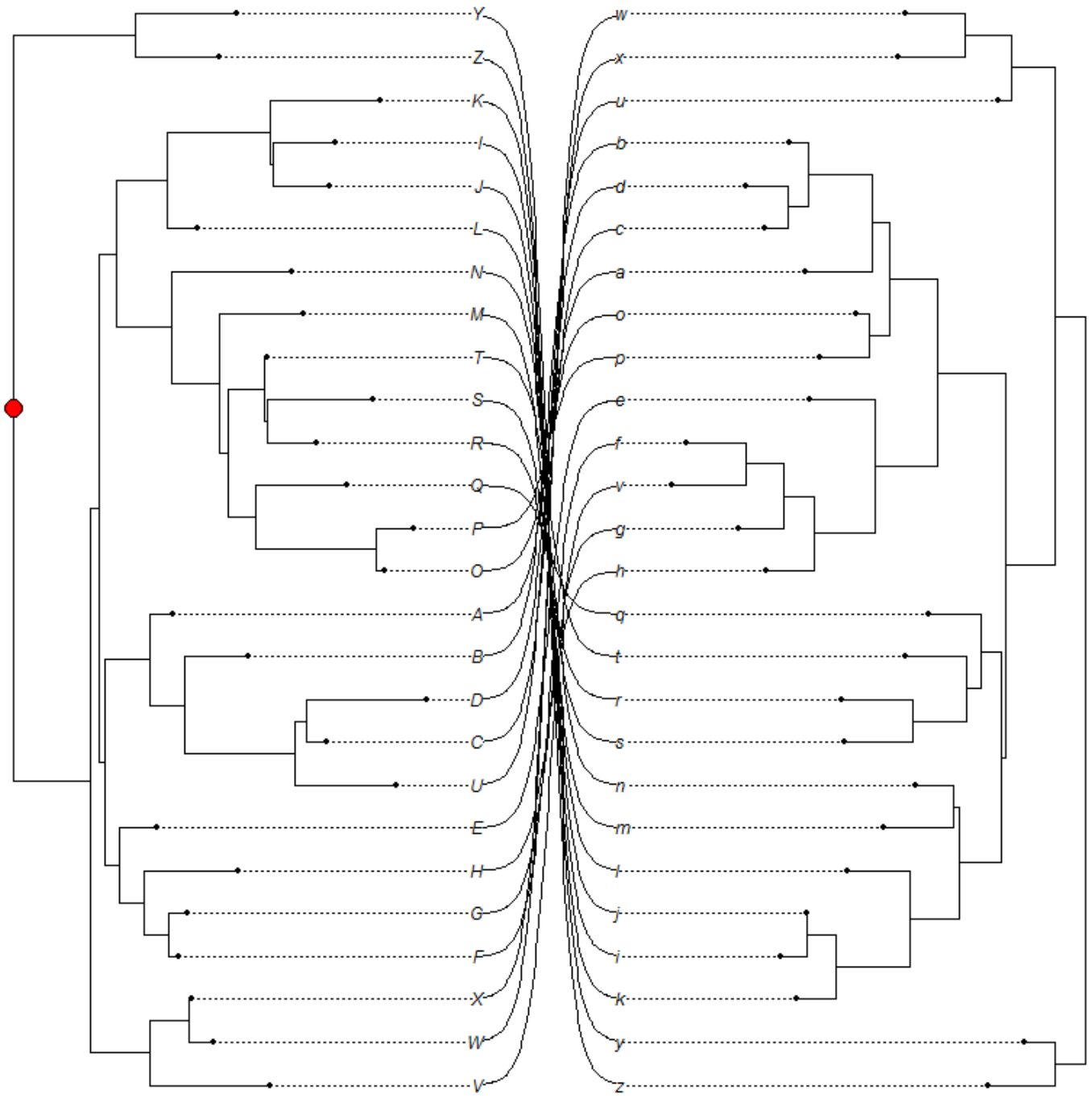
Y
Z
K
I
J
L
N
M
T
S
R
Q
P
O
A
B
D
C
U
E
H
G
F
X
W
V
w
x
u
b
d
c
a
o
p
e
f
v
g
h
q
t
r
s
n
m
l
j
i
k
y
z

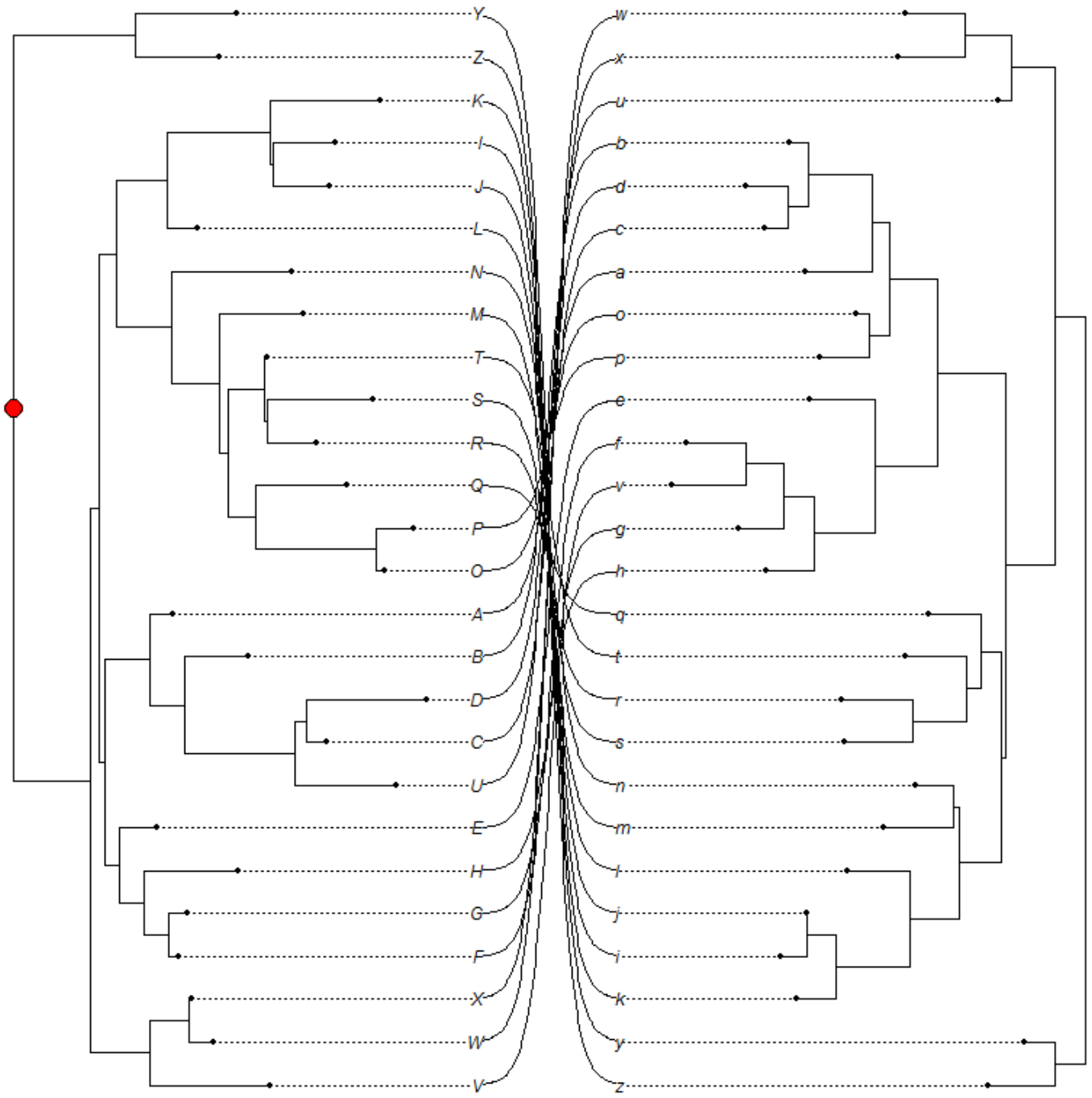
Y
Z
K
I
J
L
N
M
T
S
R
Q
P
O
A
B
D
C
U
E
H
G
F
X
W
V
w
x
u
b
d
c
a
o
p
e
f
v
g
h
q
t
r
s
n
m
l
j
i
k
y
z

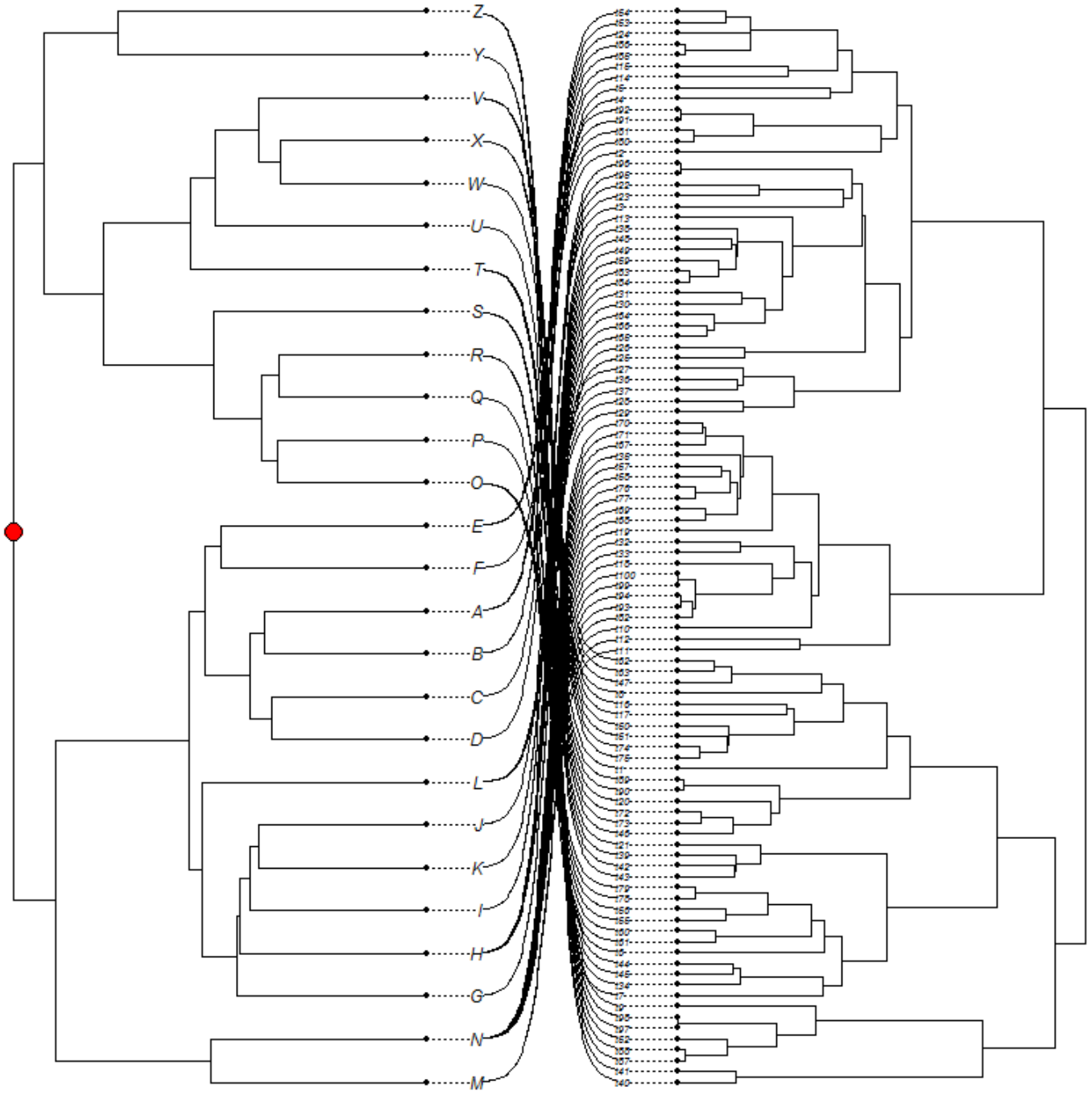
Z
Y
V
X
W
U
T
S
R
Q
P
O
E
F
A
B
C
D
L
J
K
I
H
G
N
M

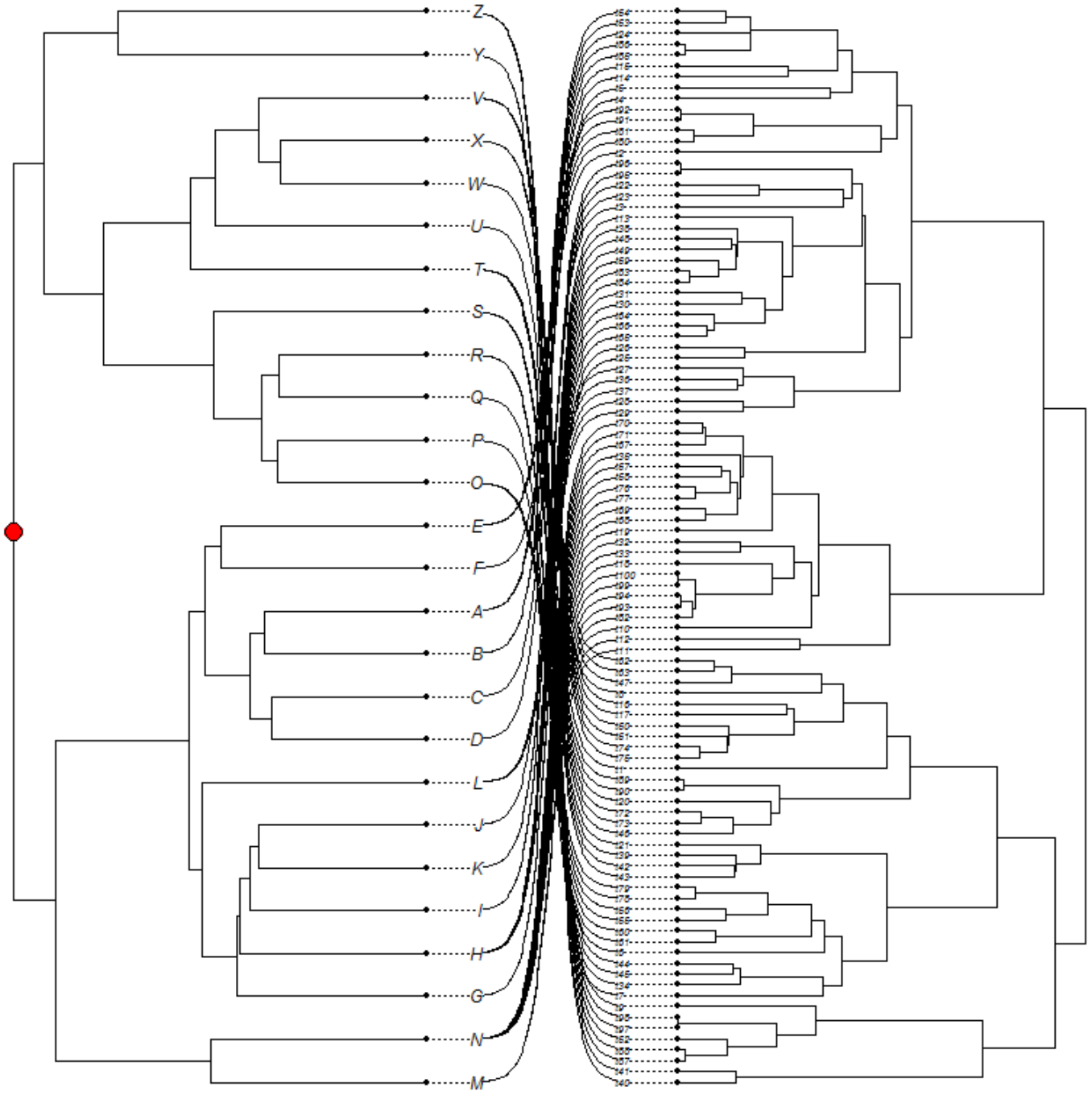
Z
Y
V
X
W
U
T
S
R
Q
P
O
E
F
A
B
C
D
L
J
K
I
H
G
N
M

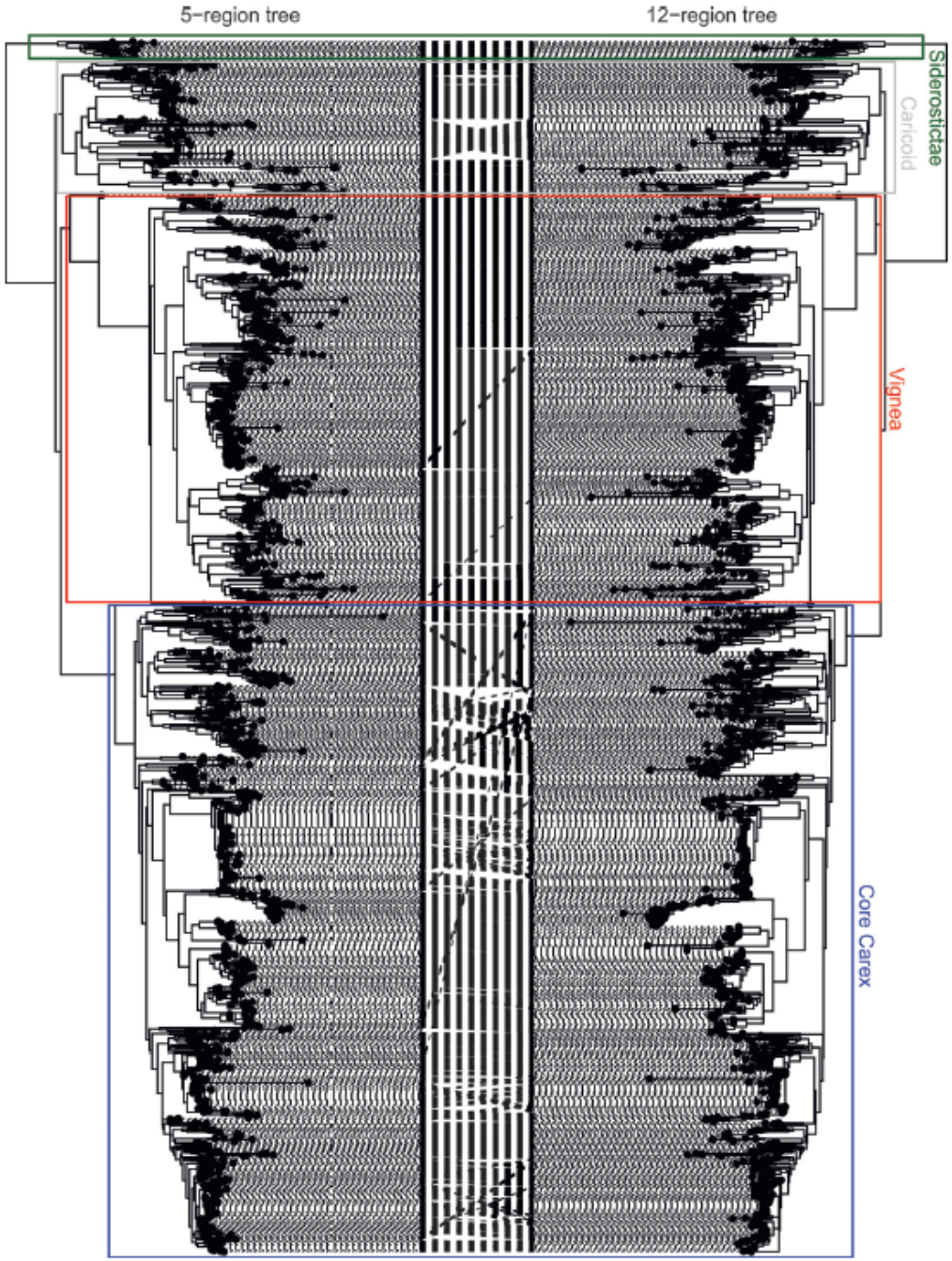

FIG. 5. 5-region phylogeny compared with 12-region phylogeny. Maximum likelihood phylogenies from the 5-region data matrix and the 12-region data matrix were pruned to shared species and plotted using the cophylo function in phytools. Lines connecting the phylogenetic trees represent shared taxa and indicate topological similarities and differences. Colored boxes indicate the major *Carex* clades.

(Pham et al. 2016; *Syst. Bot.*)

Plotting methods

- All standard statistical courses recommend plotting your data before analysis & to understand results.
- Phylogenetic data are inherently more complex, and thus require specialized visualization methods.